REPORT DOCUMENTATION PAGE

Form Approved
OMB No. 0704-0188

1. AGENCY USE ONLY *(Leave blank)*	2. REPORT DATE	3. REPORT TYPE AND DATES COVERED
	17 May 96	

4. TITLE AND SUBTITLE
Monte Carlo Simulation of Detection of Cirrus Cloud Properties By Micro Pulse Lidar

5. FUNDING NUMBERS

6. AUTHOR(S)
James A. Cotturone Jr.

7. PERFORMING ORGANIZATION NAME(S) AND ADDRESS(ES)
AFIT Student Attending:
Colorado State University

8. PERFORMING ORGANIZATION REPORT NUMBER
96-052

9. SPONSORING / MONITORING AGENCY NAME(S) AND ADDRESS(ES)
DEPARTMENT OF THE AIR FORCE
AFIT/CI
2950 P STREET, BLDG 125
WRIGHT-PATTERSON AFB OH 45433-7765

10. SPONSORING / MONITORING AGENCY REPORT NUMBER

11. SUPPLEMENTARY NOTES

12a. DISTRIBUTION / AVAILABILITY STATEMENT
Approved for Public Release IAW AFR 190-1
Distribution Unlimited
BRIAN D. GAUTHIER, MSgt, USAF
Chief Administration

12b. DISTRIBUTION CODE

13. ABSTRACT *(Maximum 200 words)*

14. SUBJECT TERMS	15. NUMBER OF PAGES 58
	16. PRICE CODE

17. SECURITY CLASSIFICATION OF REPORT	18. SECURITY CLASSIFICATION OF THIS PAGE	19. SECURITY CLASSIFICATION OF ABSTRACT	20. LIMITATION OF ABSTRACT

GENERAL INSTRUCTIONS FOR COMPLETING SF 298

The Report Documentation Page (RDP) is used in announcing and cataloging reports. It is important that this information be consistent with the rest of the report, particularly the cover and title page. Instructions for filling in each block of the form follow. It is important to ***stay within the lines*** to meet ***optical scanning requirements***.

Block 1. Agency Use Only *(Leave blank)*.

Block 2. Report Date. Full publication date including day, month, and year, if available (e.g. 1 Jan 88). Must cite at least the year.

Block 3. Type of Report and Dates Covered. State whether report is interim, final, etc. If applicable, enter inclusive report dates (e.g. 10 Jun 87 - 30 Jun 88).

Block 4. Title and Subtitle. A title is taken from the part of the report that provides the most meaningful and complete information. When a report is prepared in more than one volume, repeat the primary title, add volume number, and include subtitle for the specific volume. On classified documents enter the title classification in parentheses.

Block 5. Funding Numbers. To include contract and grant numbers; may include program element number(s), project number(s), task number(s), and work unit number(s). Use the following labels:

C	- Contract	**PR**	- Project
G	- Grant	**TA**	- Task
PE	- Program Element	**WU**	- Work Unit Accession No.

Block 6. Author(s). Name(s) of person(s) responsible for writing the report, performing the research, or credited with the content of the report. If editor or compiler, this should follow the name(s).

Block 7. Performing Organization Name(s) and Address(es). Self-explanatory.

Block 8. Performing Organization Report Number. Enter the unique alphanumeric report number(s) assigned by the organization performing the report.

Block 9. Sponsoring/Monitoring Agency Name(s) and Address(es). Self-explanatory.

Block 10. Sponsoring/Monitoring Agency Report Number. *(If known)*

Block 11. Supplementary Notes. Enter information not included elsewhere such as: Prepared in cooperation with...; Trans. of...; To be published in.... When a report is revised, include a statement whether the new report supersedes or supplements the older report.

Block 12a. Distribution/Availability Statement. Denotes public availability or limitations. Cite any availability to the public. Enter additional limitations or special markings in all capitals (e.g. NOFORN, REL, ITAR).

- **DOD** - See DoDD 5230.24, "Distribution Statements on Technical Documents."
- **DOE** - See authorities.
- **NASA** - See Handbook NHB 2200.2.
- **NTIS** - Leave blank.

Block 12b. Distribution Code.

- **DOD** - Leave blank.
- **DOE** - Enter DOE distribution categories from the Standard Distribution for Unclassified Scientific and Technical Reports.
- **NASA** - Leave blank.
- **NTIS** - Leave blank.

Block 13. Abstract. Include a brief *(Maximum 200 words)* factual summary of the most significant information contained in the report.

Block 14. Subject Terms. Keywords or phrases identifying major subjects in the report.

Block 15. Number of Pages. Enter the total number of pages.

Block 16. Price Code. Enter appropriate price code *(NTIS only)*.

Blocks 17. - 19. Security Classifications. Self-explanatory. Enter U.S. Security Classification in accordance with U.S. Security Regulations (i.e., UNCLASSIFIED). If form contains classified information, stamp classification on the top and bottom of the page.

Block 20. Limitation of Abstract. This block must be completed to assign a limitation to the abstract. Enter either UL (unlimited) or SAR (same as report). An entry in this block is necessary if the abstract is to be limited. If blank, the abstract is assumed to be unlimited.

★U.S.GPO:1990-0-273-271

THESIS

MONTE CARLO SIMULATION OF DETECTION OF CIRRUS CLOUD PROPERTIES BY MICRO PULSE LIDAR

Submitted by

James A. Cotturone Jr.

Department of Atmospheric Science

In partial fulfillment of the requirements

for the Degree of Master of Science

Colorado State University

Fort Collins, Colorado

Summer 1996

COLORADO STATE UNIVERSITY

May 17, 1996

WE HEREBY RECOMMEND THAT THE THESIS PREPARED UNDER OUR SUPERVISION BY JAMES A. COTTURONE JR. ENTITLED MONTE CARLO SIMULATION OF DETECTION OF CIRRUS CLOUD PROPERTIES BY MICRO PULSE LIDAR BE ACCEPTED AS FULFILLING IN PART REQUIREMENTS FOR THE DEGREE OF MASTER OF SCIENCE.

Committee on Graduate Work

_____

_____

_____

_____

_____
Adviser

_____
Department Head

ABSTRACT

MONTE CARLO SIMULATION OF DETECTION OF CIRRUS CLOUD PROPERTIES BY MICRO PULSE LIDAR

The development of the Micro Pulse Lidar (MPL) provides researchers with a system capable of continuous, eye-safe monitoring of atmospheric properties. The MPL operates with low energy, high pulse repetition frequency radiation in the visible portion of the spectrum. To investigate the interaction between visible radiation and atmospheric constituents, a model using Monte Carlo techniques has been refined to simulate MPL return profiles. An inherent feature of the MPL is its narrow receiver field of view (FOV) which is necessary to limit background noise. The effect of such a FOV and the role multiple scattering effects play in MPL operations are investigated in this study.

Cloud base height and the radiative properties of cirrus clouds are important for determining the radiation budget of the planet. Inferred cirrus cloud radiative properties vary with the type of crystals assumed to compose the model clouds. To properly model optically thin clouds, it is important to include a standard background atmosphere composed of Rayleigh and aerosol scatterers. Its inclusion allows one to take advantage of information deduced from both the cloud and above-cloud layer. Information that is unavailable when sampling optically thick clouds. This capability plays a pivotal role in an inversion algorithm that is developed and described. It is shown that the algorithm allows one to infer important cloud optical properties such as volume extinction coefficient, cloud optical depth, and isotropic backscatter to extinction ratio, also known as the lidar ratio. The algorithm shows that reliable results may be obtained from clouds of optical depth ranging from 0.05 to 1.4. For clouds of greater optical depth, it is shown that model "noise" causes results to become unstable. This instability is investigated and

the sensitivity of algorithm results to the accuracy of essential parameters is examined. Calculations of the multiple scattering factor are also made for model clouds of varying optical depth.

James A. Cotturone Jr.
Department of Atmospheric Science
Colorado State University
Fort Collins, CO 80523
Summer 1996

ACKNOWLEDGMENTS

I would like to express my appreciation to Dr. Thomas McKee and Dr. Chiaoyao She for sitting on the thesis committee. I would also like to thank David Wood, Sean Gillies, Andrew Heidinger, and Norm Wood for their discussion, input and friendship during this work and the United States Air Force for providing me the opportunity for graduate study.

Further, I would like to thank my advisor, Dr. Stephen Cox for his generous guidance and extend my sincere gratitude to Dr. John Davis whose expertise and advice kept me on the right path when the path was so hard to find.

Finally, I would like to thank Jennifer Dickey for her support, companionship, and love.

TABLE OF CONTENTS

Chapter 1. Introduction

Light Detection and Ranging (Lidar) systems have existed in the atmospheric science community for nearly 25 years. At a minimum, these systems have been used to gather information regarding cloud and aerosol layer heights, while more recently, techniques have been developed to decipher radiative properties such as volume extinction coefficients, optical depths and phases of cloud hydrometeors to name just a few. The use of lidar to examine the radiative effects and hence climatalogical effects of clouds and aerosols, is growing in practicality and use. As evidence, a space-based lidar system was flown on a NASA Space Shuttle mission recently as part of the Lidar In-Space Technology Experiment (LITE) (McCormick et al. 1993). It is clear that lidar's importance and capabilities are increasing with the continuing advances in laser, detector, and data reduction technologies.

Historically, lidars used in meteorological applications used radiative pulse energies with wavelengths in the visible, near-infrared, and infrared portions of the spectrum. These systems featured high energy, low pulse repetition frequency signals to conduct a multitude of cloud and aerosol measurements. Recently, these instruments have been upgraded by new solid state lasers and detectors that allow for more efficient and continuous monitoring of atmospheric properties. The Micro Pulse Lidar (MPL), as developed and outlined by Spinhirne (1993), uses design advancements that provide researchers with a small, table top, eye-safe system capable of profiling significant cloud and aerosol scattering layers, using wavelengths located in the visible portion of the spectrum. This is an important step, because for years the complexity and hazards associated with the use of a large, high energy system has plagued researchers. With the advent

of the MPL, scientists have been provided a tool which provides continuous and reliable atmospheric monitoring.

It is readily acknowledged that cirrus clouds play a vital role in the Earth's radiation budget and one of the most attractive capabilities of the MPL is its ability to continuously detect cirrus cloud properties. Traditional lidars have been used extensively to examine cirrus cloud properties (Platt 1973; Platt 1979, Intrieri and Stephens 1993). Initial tests of the MPL show that it is an effective means of conducting similar research (Spinhirne 1993). The sampling of cirrus clouds requires attention to the role Rayleigh and aerosol scatterers play in the overall backscattered energy return to the lidar whereas these scatterers are often neglected when examining clouds of greater optical depth. On the other hand, multiple scattering effects play a large role in the sampling of optically thick clouds such as cumulus but are, in some ways, just as important when examining cirrus clouds of various optical depths. The effect of multiple scattering on lidar returns has been the subject of several investigations (Kunkel and Weinman 1976; Platt 1981; Bruscaglioni et al 1995). One characteristic of the MPL is its relatively small receiver field of view (FOV) which is necessary to limit noise from background sky radiance. This has a significant effect of limiting multiple scattering contributions to returns.

Standard lidar returns contain information about the radiative properties of the remotely sampled mediums. Klett (1981) introduced a stable analytical inversion solution to determine cloud extinction coefficients from lidar returns. He showed that by selecting a reference range above cloud top level and assuming a reference extinction value, one could analytically solve for extinction coefficients throughout an atmospheric layer. A necessary assumption of Klett's algorithm is that molecular scattering could be neglected and the particulate backscatter to extinction ratio, also known as the lidar ratio, could be considered constant. Klett (1984) considered a similar solution while allowing for a variable lidar ratio. Recently, Young (1995) pointed out that when sampling high, optically thin clouds, molecular scattering could not be neglected, and presented revised methods of profiling lidar backscatter in optically thin clouds.

These methods included an intricate technique to determine the lidar ratio and applied it to an algorithm developed by Fernald (1984) which is related to Klett's original stable solution.

The purpose of this research is to (a) present a Monte-Carlo model used for simulating MPL returns, (b) provide an overview of the MPL and make comparisons to other lidar systems, (c) investigate features unique to the MPL such as wavelength and multiple scattering effects, (d) provide generalized model returns from cirrostratus clouds, (e) develop and present a simple, but effective method to determine cloud optical properties such as volume extinction profile, optical depth, and the lidar ratio.

In this work, a separate algorithm is introduced that includes molecular scattering, takes advantage of returns from both in-cloud and above-cloud, and provides a technique for determining the lidar ratio (Alvarez et al. 1993). This algorithm is summarized and a method of determining cloud extinction and optical depth is examined. The revised algorithm is tested by retrieving the optical properties of clouds that were modeled using a Monte Carlo routine simulating MPL returns. From simulated returns, the algorithm is used to infer various optical properties of the cloud including the lidar ratio.

A basic principle of laser ceilometers or lidars is that they measure cloud height by determining the amount of time it takes for a pulse of energy to travel from the transmitter to the scattering medium and back to the receiver. A cloud height is then inferred from the transit time by using the known speed of energy propagation through the medium. The expected amount of returned energy can be determined from the basic lidar equation, (Liou 1980)

$$P_r(r) = P_t \frac{A_r}{r^2} \frac{P(\pi)}{4\pi} \sigma_s \frac{\Delta h}{2} \exp[-2\int_0^r \sigma_e(r')dr']$$

where P_r is returned power, P_t is transmitted power, A_r is the receiver area or aperture, r is the range or distance to the scattering point, σ_e is the volume extinction coefficient, σ_s is the volume

scattering coefficient, and Δh is the pulse length. This equation assumes that multiple scattering effects can be neglected. Although research has shown that multiple scattering cannot be neglected at typical lidar wavelengths (Kunkel and Weinman 1976; Platt 1981; Winker and Poole 1995), this study will show that the receiver field of view associated with the MPL restricts total return to the receiver to only the lowest orders of scattering for the most optically thin cirrus clouds.

To simulate returns to the MPL, a Monte Carlo model reported by McKee and Cox (1974,1976) was revised and applied to trace the propagation of photons through the atmosphere and simulate their interaction with constituents in various model atmospheres. Large numbers of photons are traced to minimize the randomness associated with the Monte Carlo method. MPL and model atmosphere geometry are depicted in figure 1.1. The modeled cloud is located at a distance, h, from the collocated lidar transmitter and receiver. The transmitter emits energy (photons) at an elevation angle of 90° and the beam diverges with a half angle θ_t. Similarly, the receiver has a FOV half angle of θ_r. The cloud has a geometric thickness, d_c. When the standard background atmosphere is included, the height, d_{ac}, represents the geometric thickness from the top of the cloud to the upper limit of the model atmosphere such that depth of model atmosphere, $d_m = h + d_c + d_{ac}$.

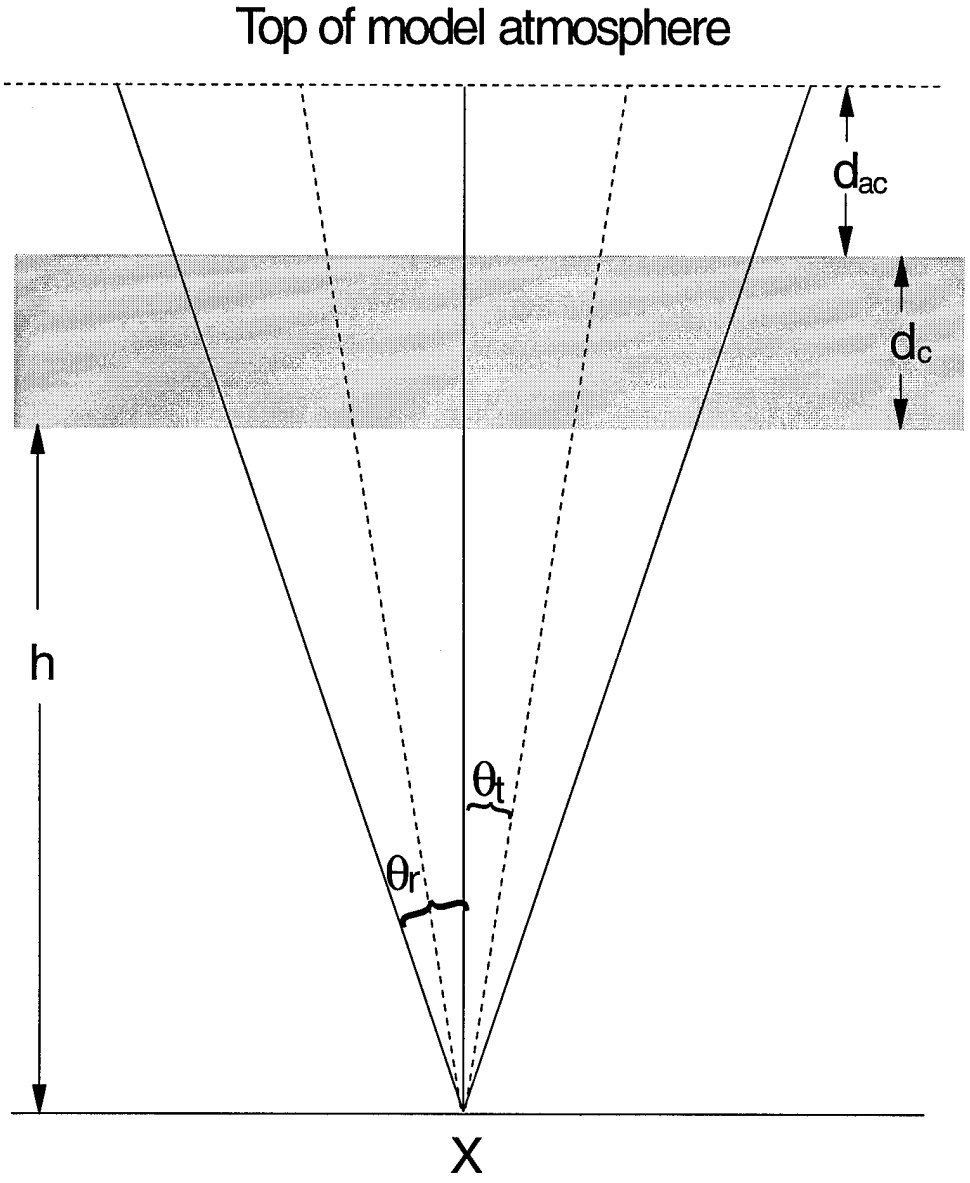

Figure 1.1 Typical MPL geometry. Transmitter and receiver are collocated at X. Transmitted beam has divergence of half angle θ_t, receiver field of view half angle is denoted by θ_r,. Model cloud is d_c thick and above cloud scattering medium is d_{ac} thick.

Chapter 2. The Monte Carlo Model

2.1 General Description

Monte Carlo modeling is used extensively in various scientific fields, including radiative transfer. It is an effective statistical approach to radiative transfer problems and has been used to model electromagnetic energy's interaction with the atmosphere. Monte Carlo models exist in a variety of forms and are defined, in part, by the direction the model traces a photon. The current model is a forward model that traces photons from the transmitter through interactions within the model atmosphere. A path ends with the photon either exiting the model geometry or after a pre-determined number of scattering events. The probability of the photon returning to the receiver is calculated at each scattering event. Monte-Carlo modeling is based on the probability of specific events occurring whose outcomes are represented by probability density functions (PDF). The techniques used here are similar to those described by Plass and Kattawar (1971) and Kunkel and Weinman (1976) and revised by Platt (1981). One difference between the current method and those upon which it is based is our inclusion of a standard background atmosphere. Whereas previous authors have chosen to neglect the effects of Rayleigh and aerosol scattering, the current work takes these factors into account. This leads to a more realistic sampling of cirrus clouds and allows us to infer optical properties from model return profiles.

2.2 Model Procedure and Application

The following model description is based on similar work reported by Keith and Cox (1994). The current model traces individual photons from the transmitter through three successive scattering events. It will be shown later that three orders of scattering provide a sufficient representation of the total return. The geometry used in the current model is shown in

figure 2.1 and is consistent with geometry used in Platt (1981). A photon is emitted from the transmitter at an angle, θ_0, which corresponds to an azimuth angle, Φ_0, such that $0 \leq \theta_0 \leq \theta_t$, where θ_t is the half angle of the transmitter beam divergence defined earlier. Every angle has an equal probability of being chosen for every photon leaving the transmitter. However, for purposes of variance reduction, θ_0 is set equal to zero in this work.

Once a photon leaves the transmitter, a scattering site along the photon path must be selected. In general, the probability that a photon will travel through a medium without an intersection is determined by

$$PROB = e^{-\tau} = \exp(-\int_0^s \sigma_e \, ds)$$

where τ is the total optical depth, σ_e is the volume extinction coefficient, and s is the distance through the medium. To find the distance along the photon path to each scattering event, a random number is chosen for PROB, the probability of a scattering or absorption event occurring, and the upper limit of integration, s, is computed. To make the model computationally more efficient, as in Platt (1981), each photon is forced to scatter within the scattering medium defined in the model input. This is done by a weighting scheme that reduces the photon's weight by a factor proportional to the optical depth remaining in the scattered direction. The probability of the photon reaching the detector, which is directly related to the backscatter energy, is appropriately reduced. The distance, S_i, from each starting point to each scattering site can then be calculated as

$$S_i = \frac{1}{\sigma_e}\left[-\ln(1 - RN(1 - T_i))\right]$$

where σ_e is the volume extinction coefficient for the photon path, RN is a random number

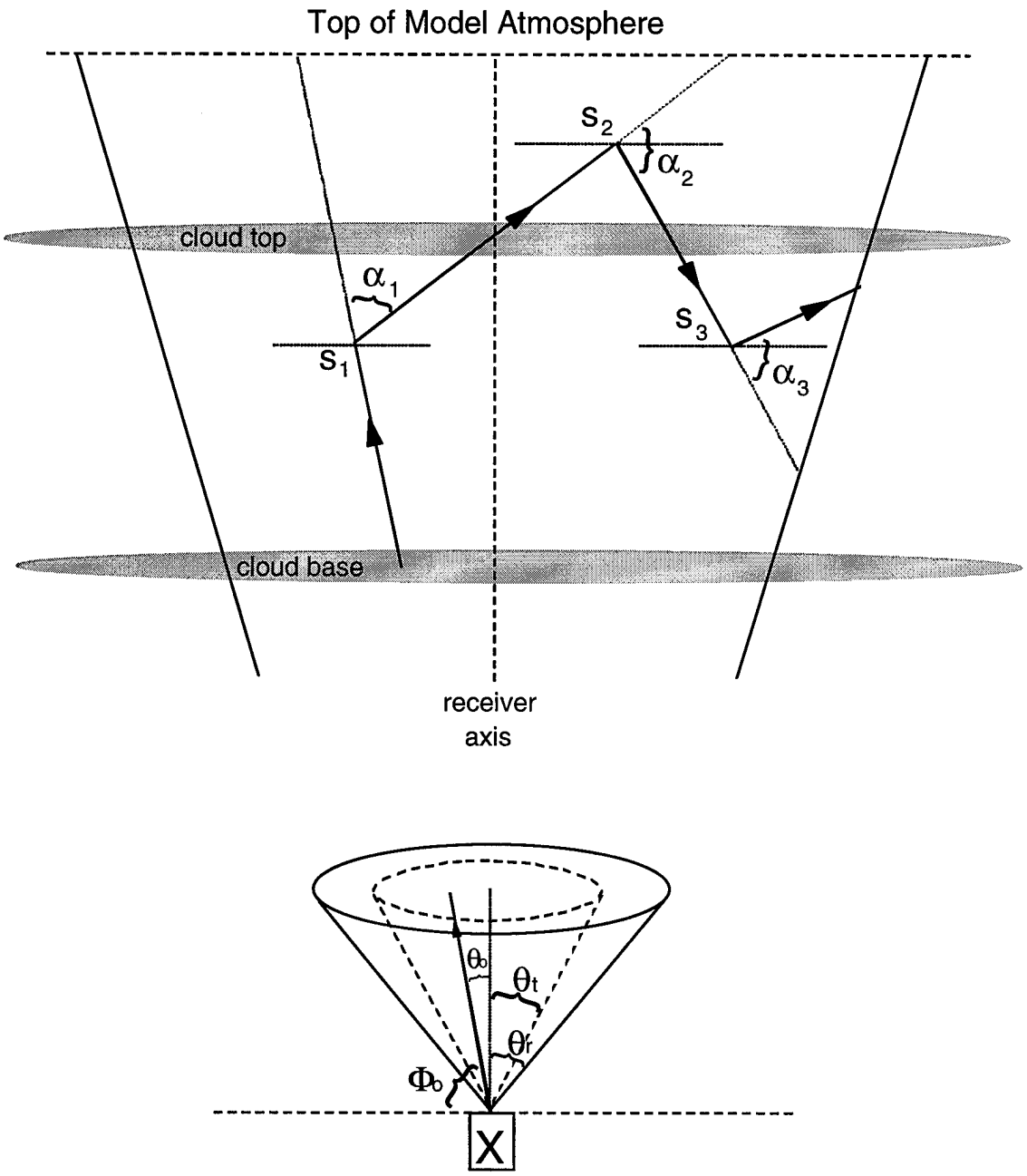

Figure 2.1 MPL and scattering geometry used in the current model. The MPL transmitter and receiver are collocated at position X. Specific geometry parameters are defined in the text.

between 0 and 1, and T_i is the transmittance from the current location to the user defined model boundary in the photon's current direction.

The type of scattering event is then determined and its applicable phase function is used in the calculations that follow. Rayleigh, aerosol, and cloud hydrometeor scatterers can all be included in the model. The type of scatterer is determined pseudo-randomly, weighted according to each scatterer's contribution to the total volume extinction coefficient. Rayleigh and aerosol concentrations and extinctions used in this model are based on the published tables of Elterman (1968). The phase function for aerosol scattering is approximated by the phase function for Haze L defined by Diermendjian (1969) and calculated from Mie theory.

At each scattering site, the probability of a photon returning directly to the receiver is represented by

$$PR = [\frac{A_e P(\psi)}{Z^2}] W_n \omega_0{}^n e^{[-\tau_e]}$$

where A_e is the effective receiver aperture, $P(\Psi)$ is the applicable single scattering phase function for angle Ψ, Z is the distance from the scattering point to the receiver, ω_0 is the single scattering albedo of the medium, τ_e is the effective optical depth from the scattering site to the height of the receiver, and n is the order of scatter. W_n is the weighting factor which compensates for forcing the scatters to occur within the scattering media, and is represented as

$$W_n = (1 - T_n) W_{n-1}$$

where T_n is the transmittance to the model boundary.

At each scattering site, a new direction is determined by selecting a random scattering angle, α_n, defined as the angle between the incident direction vector and the new scattered direction vector, within the plane of the two vectors. The random angle is selected based on the

normalized single scattering phase function of the scattering medium. The new azimuthal direction, determined from the photon's frame of reference, is then selected from a uniform distribution between 0 and 2π.

Each photon is tracked through three scattering events and probabilities for each are computed. The sum of the probabilities for all photons, as a function of height and order of scattering, is maintained and after all photons are processed, the model determines the overall probability of a photon returning to the receiver from each designated range gate height.

2.3 Statistical Convergence

Model output was tested to ensure statistical convergence. Initially, statistics were examined considering the cirrostratus cloud as the only constituent of the scattering medium. In the next section, the effects of Rayleigh and aerosol scattering will be considered. A total of **N** photons divided into 10 equal sets are processed in each run. From each set, a mean scattering probability for each order of scattering is determined. Later, analysis will show that for typical cirrus cloud optical depths, first order scattering contributes over 97 percent of the total returned energy. Therefore, when examining the statistical reliability of the model, only first order scattering statistics are considered.

The variance of each run is defined as

$$\sigma^2 = \sum_{i=1}^{M} \frac{(x_i - \mu)^2}{M}$$

where x_i is the mean scattering probability for each set, μ is the mean scattering probability for the entire run and M is the number of sets in each run. Results were obtained by modeling a homogeneous 1 km thick cirrostratus cloud composed of randomly oriented hexagonal ice crystals with an extinction coefficient of 0.386 km^{-1} located 7 km above the lidar. Initially, no Rayleigh or background aerosol extinction is present and a total of 1 million photons are

processed. A sample of the variance for each model run as a function of number of photons per set is given in figure 2.2. The curve illustrated is in agreement with the central limit theorem of statistical probability which states that the convergence of the runs improves according to $1/N^{1/2}$. The normalized standard error was also calculated for each run and is defined as

$$ERR = \frac{\sigma}{\mu}$$

where σ is the standard deviation.

Figure 2.3 shows the standard error as a function of number of photons per set for the modeled cirrostratus cloud. The graph shows that cirrostratus returns with no standard atmosphere are statistically well behaved based on the relatively small standard error.

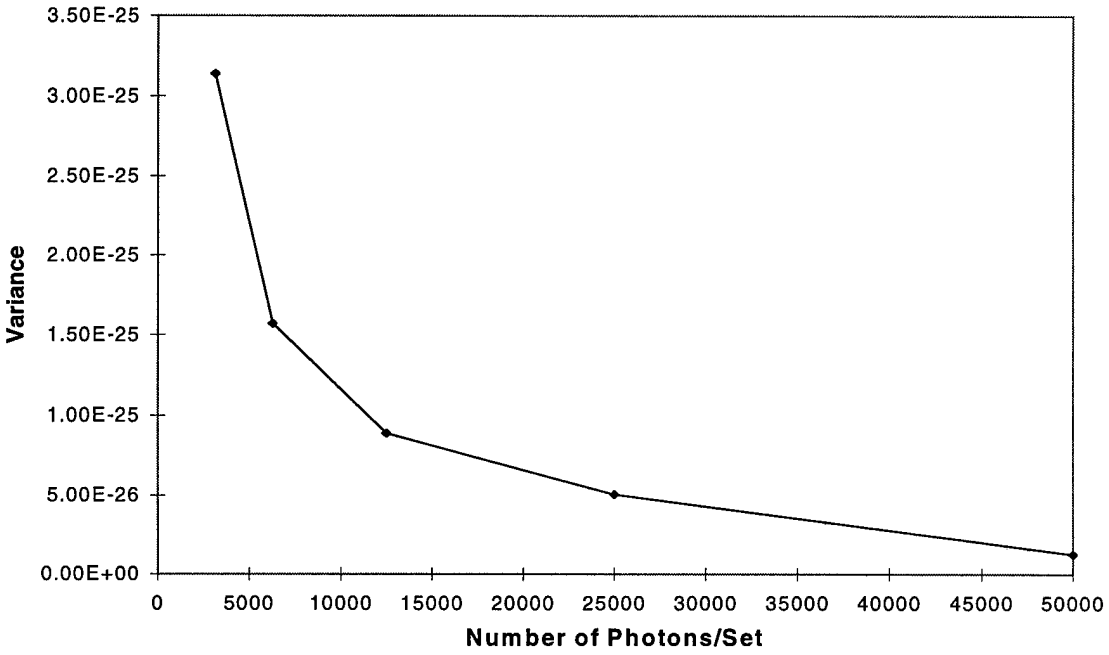

Figure 2.2 Variance of the mean scattering probability as a function of number of photons per set. A total of 10 sets were processed for each model run. Scattering media is 1 km thick cirrostratus cloud composed of hexagonal crystals located 7 km over lidar. No background atmosphere is present.

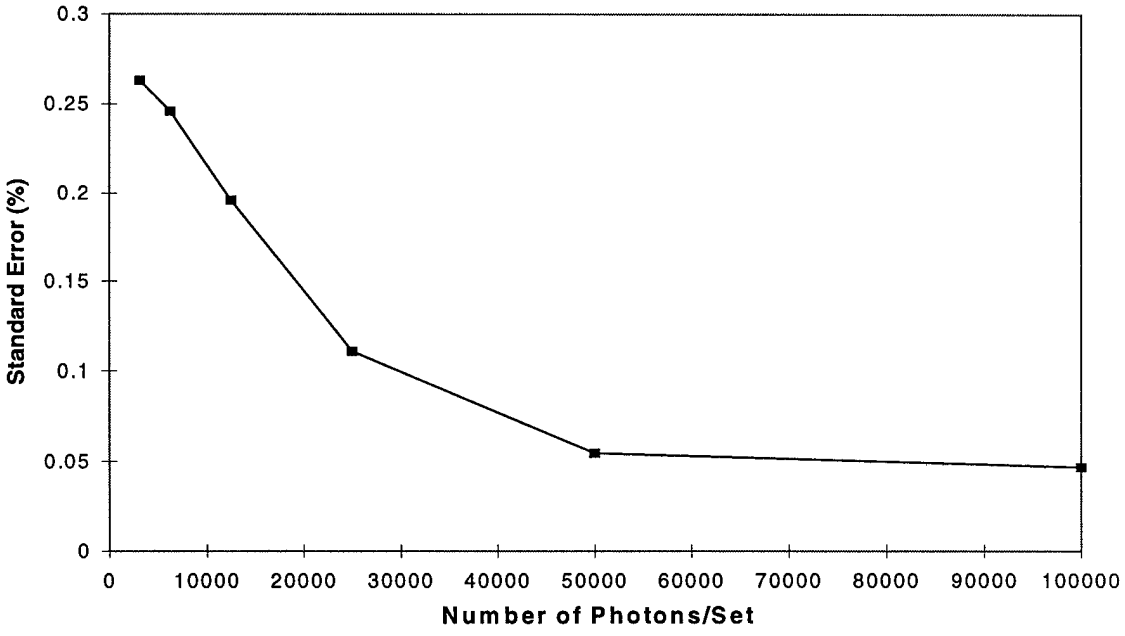

Figure 2.3 Standard error as function of number of photons per set for 1 km thick homogeneous cirrostratus cloud composed of hexagonal crystals located 7 km above the lidar. No background atmosphere is present.

2.3.1 Effect of Standard Atmosphere on Model Statistics

The inclusion of a standard atmosphere significantly impacts the statistical behavior of the model. A model cirrostratus cloud was placed at a height of 7 km in a standard atmosphere consisting of Rayleigh and aerosol scatterers allowing interactions in the above-cloud, cloud, and subcloud regions. Figure 2.4 shows the variance of the model return as in figure 2.2, but with a subcloud standard atmosphere region present. The variance in the model results including Rayleigh and aerosol scatterers is significantly greater than in the case with no standard atmosphere. A physical explanation for this may exist in the greater number of potential scatterers in a standard atmosphere compared to the number of scatterers when only the cloud is present. A finite number of photons distributed over more scatterers causes an increase in the statistical error. Hence, figure 2.5 shows significantly higher standard errors as a function of number of photons per set. These results show that in the presence of a subcloud background atmosphere, the processing of significantly more photons is required in order to reduce the standard error to statistically acceptable levels. This fact must be taken into account when considering results derived from model runs that include a standard atmosphere. All results discussed below, which include a standard background atmosphere, are the result of processing 1 million photons per set (10 million total). Results show that for a run consisting of 10 million photons the standard error is approximately 5 percent. This is a pragmatic choice of the number of photons, given that the processing of additional photons leads to an unacceptable increase in computer run-time.

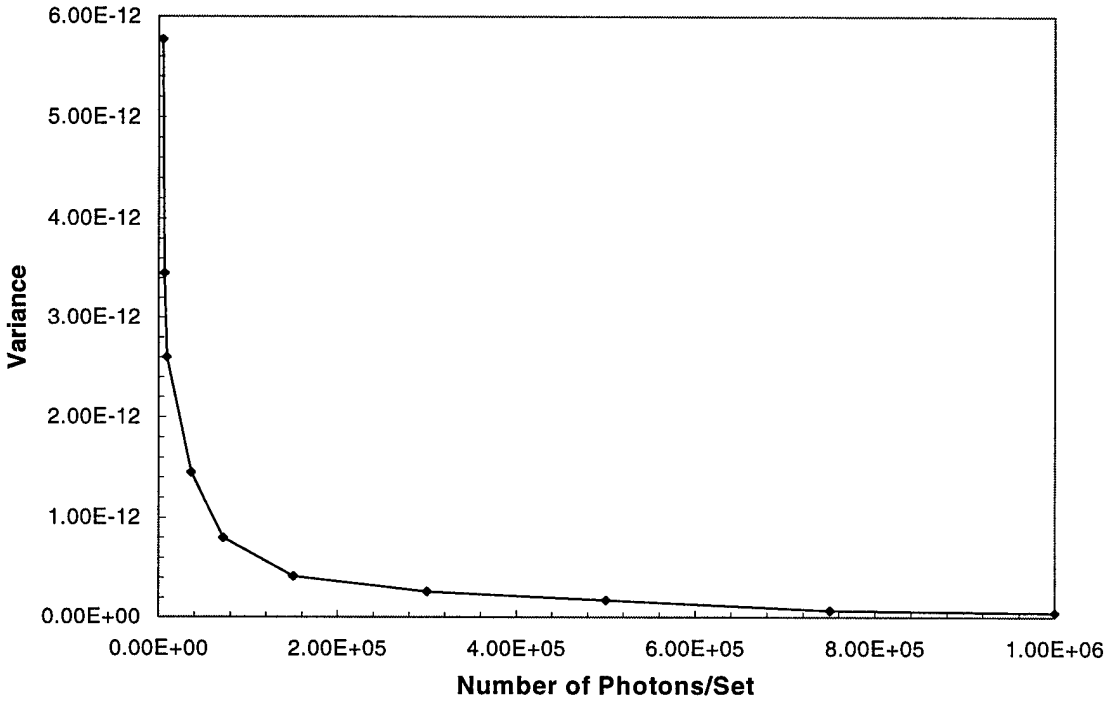

Figure 2.4 Same as in figure 2.2, except for presence of Rayleigh and aerosol scattering.

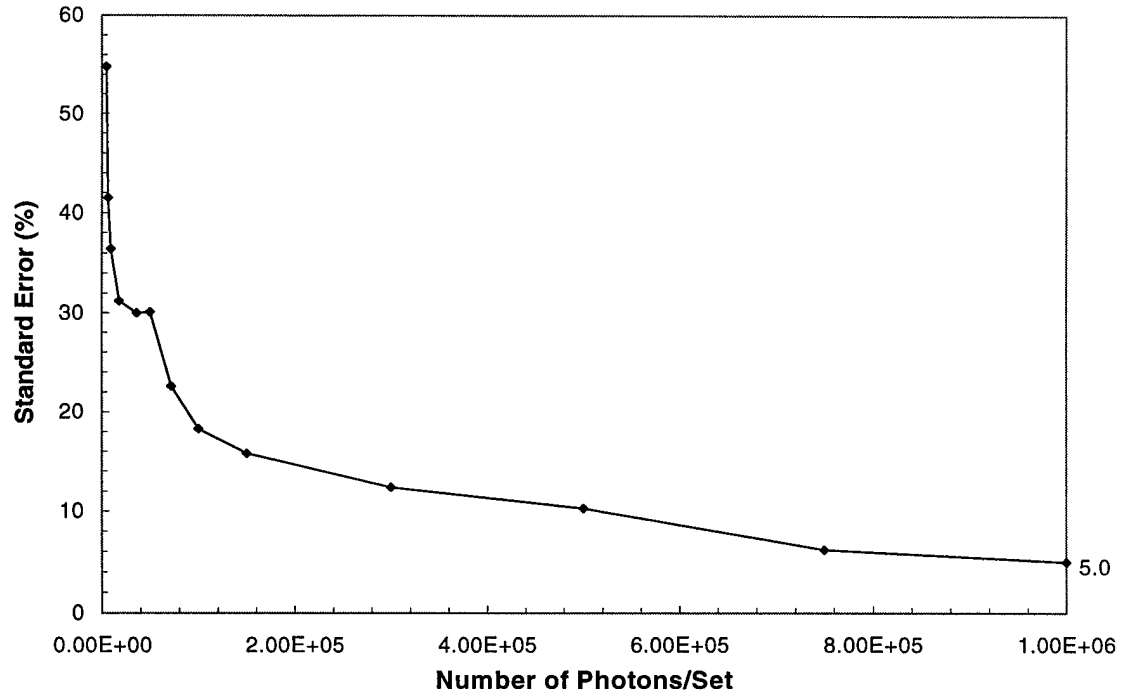

Figure 2.5 Same as in figure 2.3, except for presence of Rayleigh and aerosol scattering.

Chapter 3. Micro Pulse Lidar

3.1 General Discussion

The MPL provides users with capabilities previously unavailable to researchers. It was designed with the goal of developing a system that is capable of continuous eye-safe use while having the sensitivity to detect all significant cloud and aerosol scattering layers. Also, it needed to be sufficiently user friendly to be operated by non-specialists. A brief overview of the MPL and its differences from more standard systems is given below with a complete discussion available in Spinhirne (1993).

3.2 General description and comparison with other Lidar systems

There are three basic differences between the MPL and conventional lidar systems. First, the laser pulse repetition frequency (PRF) is much higher and the pulse energies much lower in the MPL. It is this low pulse energy expanded to fill the 20 cm transmitting aperture, thus lowering the energy density, that permits the system to be eye-safe. Secondly, the solid state lasers are diode pumped rather than flashlamp pumped and are much more efficient and smaller. This results in system power requirements on the order of tens of watts rather than hundreds of watts for a nominal one watt of transmitted power. The third difference is that the signal detector is a solid state Geiger Avalanche Photon Diode, photon-counting detector rather than a photo multiplier detector. The advantage of this is that photon counting offers much higher quantum efficiency and is generally a more accurate and problem free means of signal acquisition for low level signals than is analog detection.

An example of the basic differences between the MPL and the more conventional lidars is provided in table 3.1. System specifications are given for the MPL as well as lidars used in the LITE and experimental cloud lidar pilot study (ECLIPS) programs as described by McCormick et al. (1993) and Carswell et al. (1995), respectively. All systems operate in the visible portion of the spectrum. Notice the major difference in energy levels between the MPL and the lidars used in the two experiments. Although this low energy level allows the MPL to be eye-safe, it does, in general, decrease the signal to noise ratio. It also makes it nearly impossible to detect stratospheric aerosol during daylight hours due to background radiative energy. To help limit background noise in the MPL, the smallest possible receiver FOV is necessary. It will be shown later, that this small receiver FOV significantly limits multiple scattering effects. Even with the MPL's low pulse energy levels, laser beam expansion is used to meet eye safety requirements. Therefore, beam expansion and collimation by a telescope is required. With a pulse repetition frequency (PRF) of 2,500 Hz, a pulse of energy travels approximately 120 km at the speed of light before the next pulse is emitted. Therefore, if it is assumed that only the lowest orders of scattering contribute significantly to the overall return, multiple trip echoes do not play a significant role in MPL operations.

	MPL	LITE	ECLIPS
Wavelength (nm)	523	532	532
Pulse Energy (μJ)	20	4.6×10^5	5.0×10^5
Receiver FOV (mrad)	0.1	1.1 or 3.5	---------
PRF (Hz)	2500	10	20

Table 3.1 Comparison of lidar specifications between MPL and lidar systems used in the LITE program and the ECLIPS experiment. Note that comparison specifications are for 532 nm wavelength although comparison systems have multi-wavelength capabilities.

3.3 Multiple Scattering Contributions to MPL Returns

The current model was used to investigate the importance of multiple scattering in MPL returns. Other authors have examined the effect of multiple scattering on the overall return signal. Bruscaglioni et al. (1995) showed that the contribution from higher orders of scattering was highly dependent on receiver FOV. In their work, they examined the ratio of return from multiple to single scattering at various depths in a C.1. model cloud (Deirmendjian 1969). Winker and Poole (1995) examined multiple scattering effects for both ground-based and space-based lidars. They concluded that multiple scattering plays a much greater role for space-based than for ground-based lidars, due mainly to the larger diameter of the receiver footprint on a cloud for the space-based systems.

Using the current model, a similar analysis was conducted using a homogeneous cirrostratus cloud located 7 km above the lidar. No standard atmosphere was present. Model input variables included a cloud volume extinction coefficient of 0.386 km^{-1}, pulse wavelength of 0.55 μm, single scattering albedo of unity and receiver FOV set to 0.1 mrad, 1 mrad, and 10 mrad. A total of one million photons was modeled for each run.

Figures 3.1, 3.2, and 3.3 show results of model runs using receiver FOVs of 0.1, 1, and 10 mrad, respectively. The two curves in each graph represent the ratio of double to single scattering and the ratio of multiple to single scattering. Results are given for the entire depth of the 1 km thick cloud. Note that the ordinates in each graph differ. The difference between curves shows the contribution from orders of scattering greater than two. Although the impact of multiple scattering increases the farther into the depth of the cloud, its contribution remains comparatively small. For receiver FOV of 10.0 mrad, the sum of the orders greater than one contributes as much as 25 percent of the total return to the receiver. For FOV equal to 0.1 mrad, higher orders contribute less than 5 percent of the total return. This is further illustrated in figure

3.4 that shows the cumulative density functions for the three model runs calculating total return probability for each order of scattering. Given these results and the MPL's FOV of 0.1 mrad, model runs in this work are limited to 3 orders of scattering and the relatively minimal returns from higher order scattering are neglected.

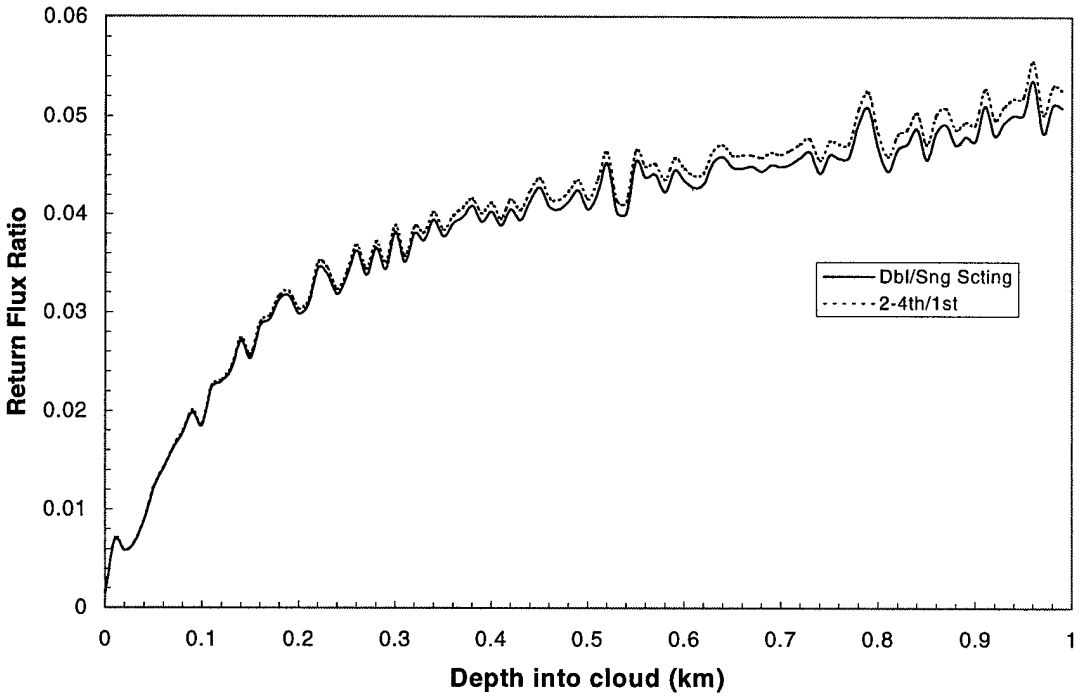

Figure 3.1 Ratio of multiple scattering contribution to single scattering contribution to lidar return. Results for **receiver FOV = 0.1 mrad**, H=1 km, using a homogeneous cirrostratus cloud composed of randomly oriented hexagonal ice crystals with $\sigma_{ext} = 0.386\ km^{-1}$. No background atmosphere is present.

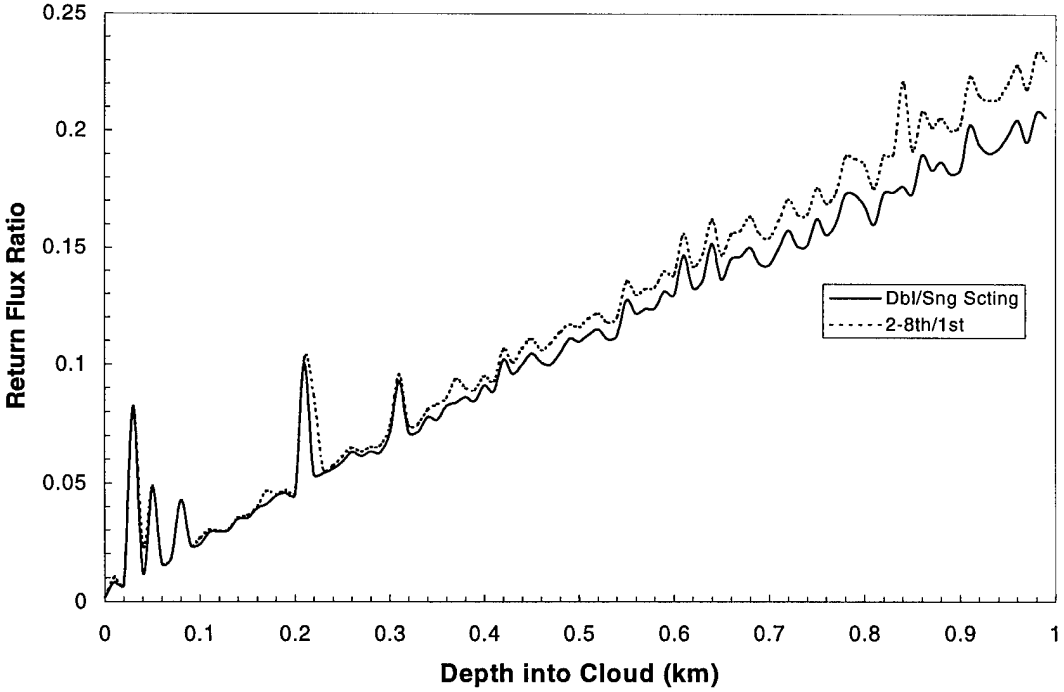

Figure 3.2 Same as figure 3.1 except **receiver FOV = 1.0 mrad**.

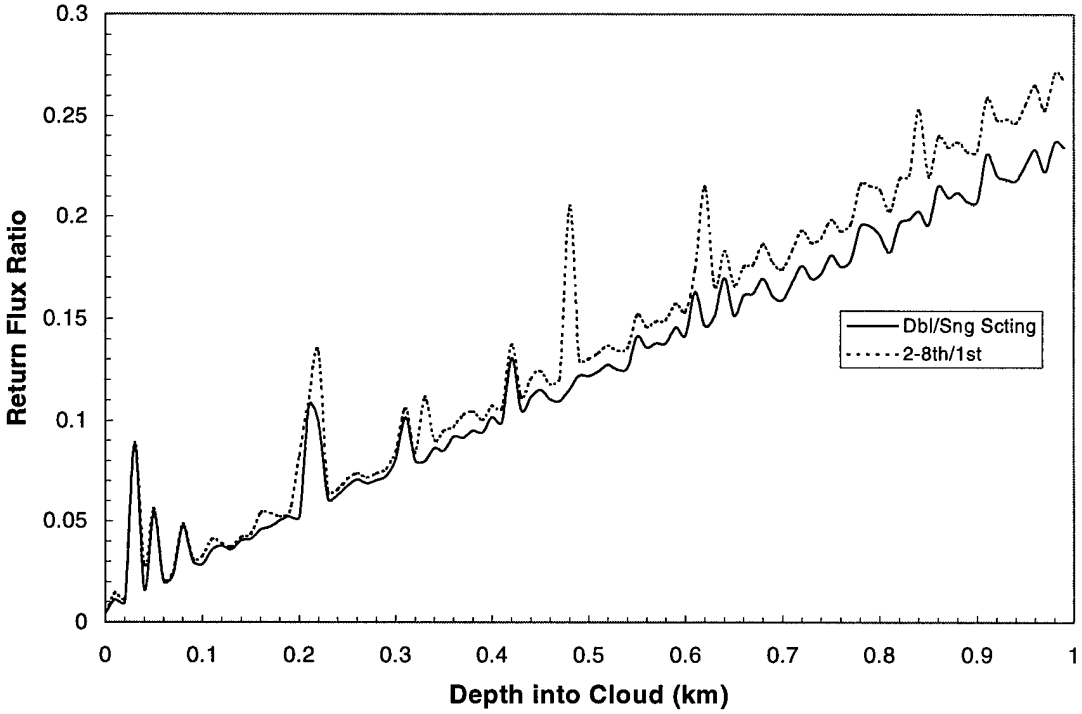

Figure 3.3 Same as figure 3.1 except **receiver FOV = 10.0 mrad**

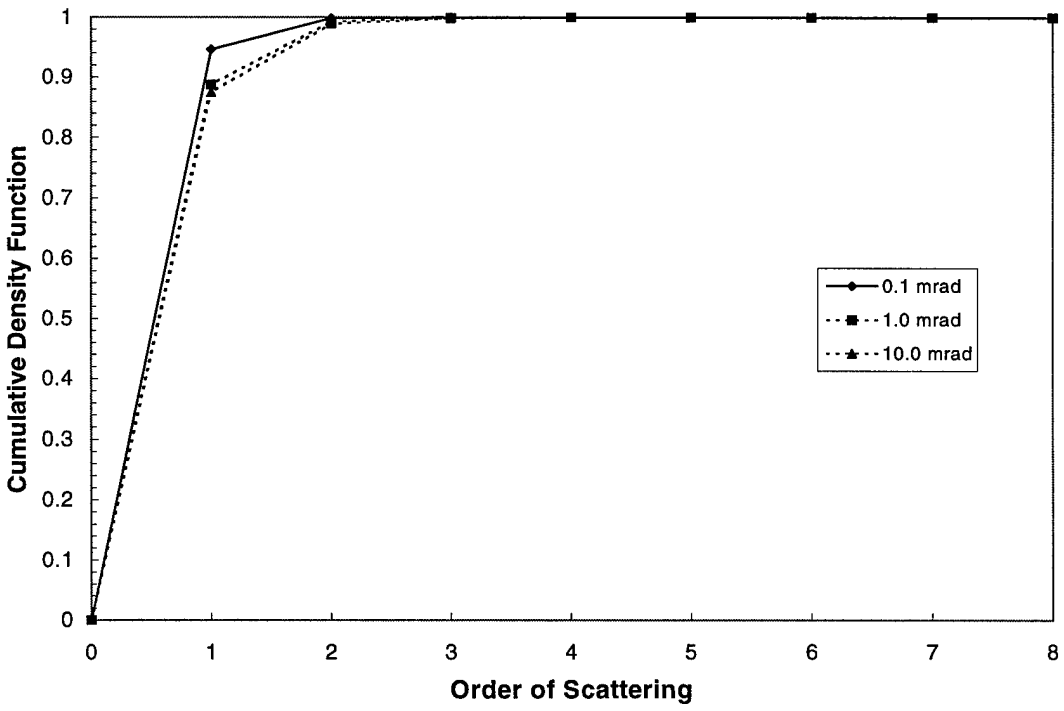

Figure 3.4 Cumulative density function showing the summation of the total contribution from each order of scattering for all three receiver FOVs.

Chapter 4. Lidar and Atmospheric Media Parameters

4.1 General Discussion

Specific initialization parameters are required to produce the model results presented in this work. The Monte Carlo model simulates the atmospheric propagation of photons emitted from the MPL based on a number of initializations which can be loosely broken down into hardware configurations and scattering media property parameters. In addition, several assumptions are made to improve the performance and statistical reliability of model results.

In all model runs, a wavelength of 0.55 μm is used to approximate the MPL's actual operational wavelength of 0.523 μm. The approximation is necessary to accommodate other initialization parameters such as single scattering phase functions and volume extinction coefficients that are calculated and published at the 0.55 μm wavelength. This approximation has minimal impact on the simulation and evaluation of the lidar's performance. In all model runs, a vertically pointing lidar is assumed. In the model, the assumed pulse width of the transmitted energy results in each range gate having a width of 10.0 meters. The MPL's transmitter and receiver are collocated and located 1 m above ground level, which is 100 m above mean sea level. The modeling in this work is designed only to simulate MPL returns in general and not its performance in a specific geographical location. The receiver FOV and transmitter beam divergence are set to 0.1 and 0.0 mrad, respectively.

Two types of scattering media besides Rayleigh scattering were designated for each model run. These consisted of background aerosol and the cirrostratus cloud being modeled. The height and thickness of the cloud are specified and placed in a background standard

atmosphere composed of Rayleigh and aerosol scatterers with concentrations and optical properties provided by Elterman (1968). The single scattering phase function, $P(\Psi)$, and the volume extinction coefficient, σ_e, for the background aerosol were derived from Mie theory calculations based on the Haze L properties defined by Diermendjian (1969). In all calculations, single scattering albedo is assumed to be unity. Cirrus cloud properties are taken from Takano and Liou (1989) and follow their randomly oriented hexagonal ice crystal approximation calculations for a cirrostratus cloud. Figure 4.1 shows the phase functions for both Haze L and hexagonal crystals that comprise the cirrostratus cloud.

4.2 Effect of Lidar Wavelength

Historically, lidars have been operated at a variety of wavelengths. Much work has been done modeling laser ceilometer and lidar performance using the near Infrared wavelength of 0.90 μm. Keith and Cox (1994) used a similar version of the current model to simulate performance of a laser ceilometer operating at 0.901 μm. They showed that certain atmospheric conditions could have adverse effects on the ceilometer's ability to detect clouds. Their findings could be applied similarly to lidars operating at a visible wavelength. Lidars used during the ECLIPS and LITE experiments both operated at a wavelength of 0.532 μm. Similarly, the MPL operates at a wavelength of 0.523 μm.

Monte Carlo modeling simulates the interaction between electromagnetic pulse energy, and the medium through which it propagates based on the histories of millions of photons. In the current model, the probability a scattering event occurring is calculated and based on single scattering properties of the scatterers selected along the photon path. The nature of these interactions and ultimately the performance of the instrument is partly dependent on the wavelength of the pulse energy emitted by the lidar.

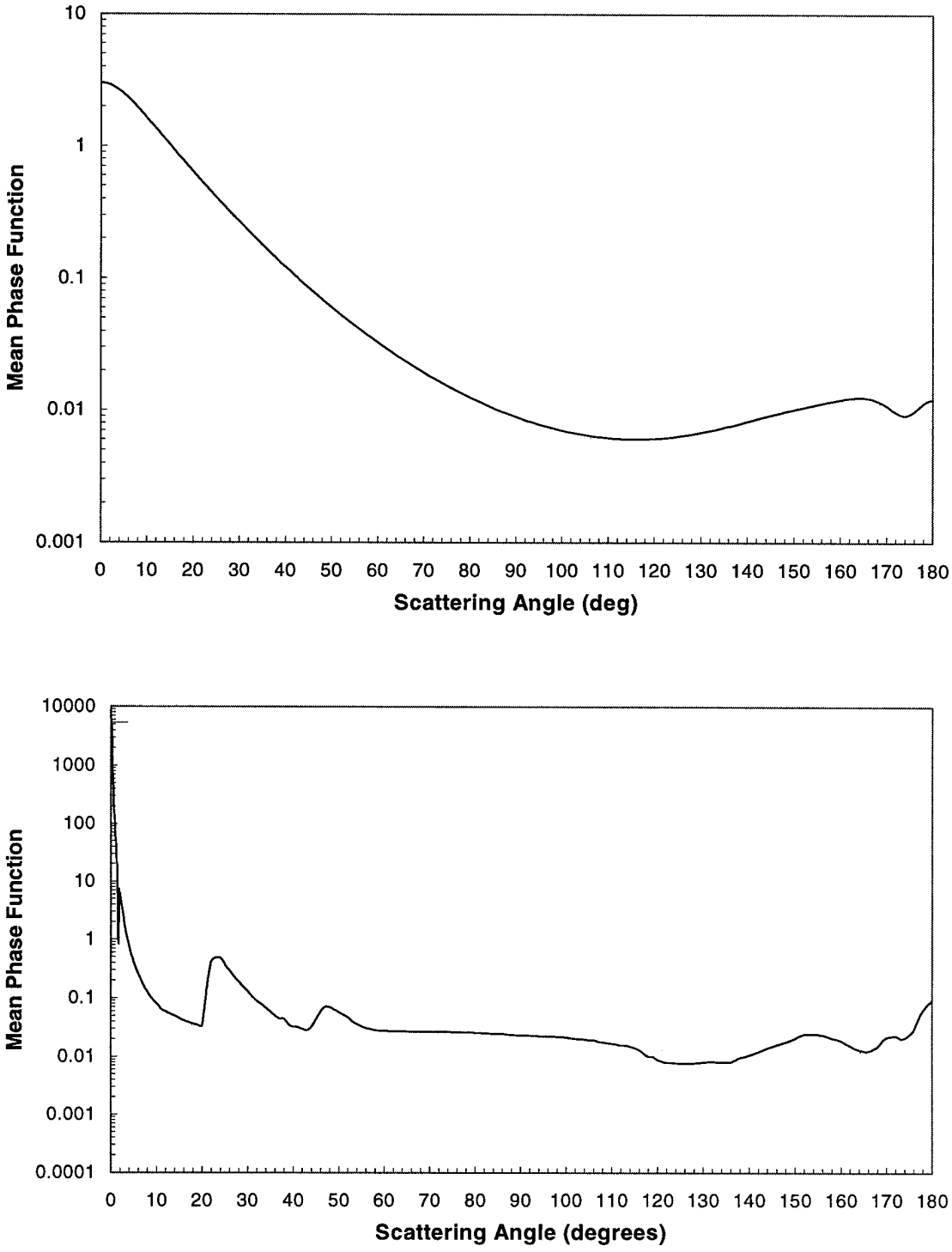

Figure 4.1 Phase Functions, P(Ψ), as a function of scattering angle, for Haze L, used to approximate aerosol scattering (top) and hexagonal crystals that comprise modeled cirrostratus cloud (bottom).

Particle single scattering properties and atmospheric radiative properties vary with pulse energy wavelength. The volume extinction coefficient of the scattering medium is dependent on wavelength. Table 4.1 shows volume extinction coefficients of both background aerosol and Rayleigh scatterers for a series of 1 km layers. The table demonstrates that extinction due to background levels of Rayleigh and aerosol scatterers is highly wavelength dependent. Single scattering phase functions are also dependent on wavelength. The phase function for background aerosol scatterers was approximated by the single scattering phase function for Haze L. Figure 4.2 compares Haze L phase functions derived from Mie theory as a function of scattering angle at 0.55 and 0.90 μm. A significant feature of this comparison is the peaked forward and backward scattering at 0.55 μm. This increases the probability of photons remaining in the receiver FOV and eventually returning to the receiver, thus causing an increase in the subcloud extinction and decreasing the detectability of the cloud.

Height	Rayleigh		Aerosol		Total Extinction	
(km)	$\lambda = 0.55$	$\lambda = 0.90$	$\lambda = 0.55$	$\lambda = 0.90$	$\lambda = 0.55$	$\lambda = 0.90$
0	1.16×10^{-2}	1.58×10^{-3}	1.58×10^{-1}	1.20×10^{-1}	1.70×10^{-1}	1.22×10^{-1}
1	1.06×10^{-2}	1.44×10^{-3}	6.95×10^{-2}	5.28×10^{-2}	8.01×10^{-2}	5.42×10^{-2}
2	9.55×10^{-3}	1.30×10^{-3}	3.00×10^{-2}	2.28×10^{-2}	3.96×10^{-2}	2.41×10^{-2}
3	8.63×10^{-3}	1.18×10^{-3}	1.26×10^{-2}	9.57×10^{-3}	2.12×10^{-2}	1.07×10^{-2}
4	7.77×10^{-3}	1.06×10^{-3}	6.66×10^{-3}	5.06×10^{-3}	1.44×10^{-2}	6.12×10^{-3}
5	6.99×10^{-3}	9.51×10^{-4}	5.02×10^{-3}	3.81×10^{-3}	1.20×10^{-2}	4.76×10^{-3}
6	6.26×10^{-3}	8.53×10^{-4}	3.54×10^{-3}	2.59×10^{-3}	9.80×10^{-3}	3.44×10^{-3}
7	5.60×10^{-3}	7.62×10^{-4}	3.29×10^{-3}	2.50×10^{-3}	8.89×10^{-3}	3.26×10^{-3}

Table 4.1 Extinction coefficient values taken from Elterman (1968). Units of extinction are km^{-1} and wavelengths are in microns.

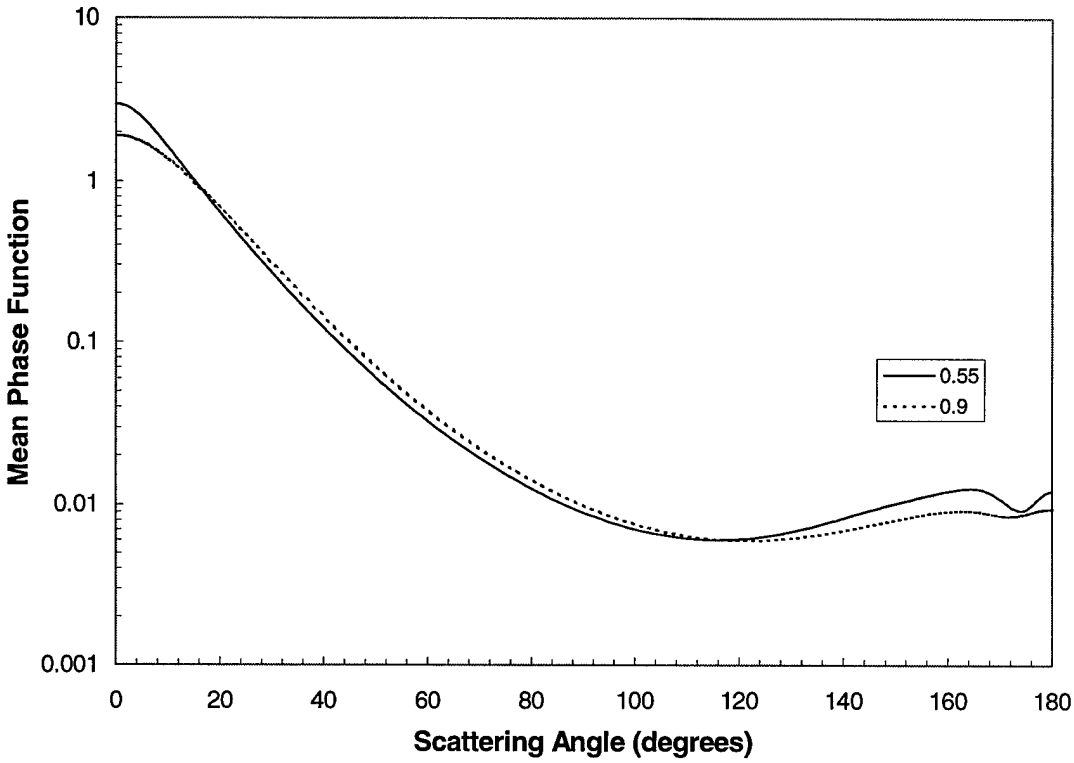

Figure 4.2 Wavelength comparison of mean phase functions as a function of scattering angle for Haze L.

Data shows the overall probability of return (return flux) is greater for the 0.55 μm wavelength at all levels. It is concluded that operating at 0.55 μm leads to more subcloud extinction than at 0.90 μm. This results in a relative decrease in cirrus returns due to their high altitude, particularly in highly turbid atmospheres.

4.3 Effect of Ice Crystal Characteristics

To model lidar returns from cirrus clouds, one must have an understanding of the microphysical structure of the ice crystals that make up the cloud. The strong influence of crystal size, shape, and orientation on the character of the phase function will have significant impact on the radiative properties of various ice clouds. Although the non-sphericity of cirrus crystals is widely acknowledged, for radiative transfer calculations, nonspherical ice crystals have been approximated by spherical particles (Plass and Kattawar 1968). It is no surprise that this simplification has been questioned. Crystals sampled in clouds at temperatures below -25° C have been found to be mainly hexagonal (Platt 1981). The clouds modeled in this work are 7 km in height and are assumed to be below this temperature. Several attempts to develop applicable cirrus crystal phase functions have been reported. Huffman (1970) developed a phase function for plates and irregular columns. Liou et al. (1976) and Sassen and Liou (1979) measured the phase function for ice needles, columns, and plates. Jacobowitz (1971) computed, by ray-tracing methods, the scattering from hexagonal crystals which were assumed to be randomly oriented in one plane. More recently, Takano and Liou (1989) developed a more exact phase function for randomly orientated hexagonal ice crystals and further emphasized the limitations of the spherical approximation. The phase function presented by Takano and Liou is used to represent scattering by cirrostratus crystals throughout this work.

For purposes of comparison, figure 4.3 provides the mean single scattering phase function for both hexagonal crystals and the spherical approximation. The spherical phase function is derived from a separate Mie code calculation. Notice the typical rainbow at 138° in the spherical approximation curve, while the 22° halo, which is indicative of hexagonal crystals and often observed in nature, is evident in the hexagonal approximation curve. More subtle differences include a higher value for total forward scattering (0°) in the spherical and a substantially higher backscatter for the hexagonal approximation.

Figure 4.4 shows the effect of the different phase functions on total return flux. The model run was for a 1 km thick cirrostratus cloud with an optical depth of 0.386 located 7 km directly above lidar in the presence of a standard background atmosphere. The use of the hexagonal instead of spherical approximation results in an increased return of energy to the lidar primarily due to the hexagonal crystal's increased backward peaked phase function.

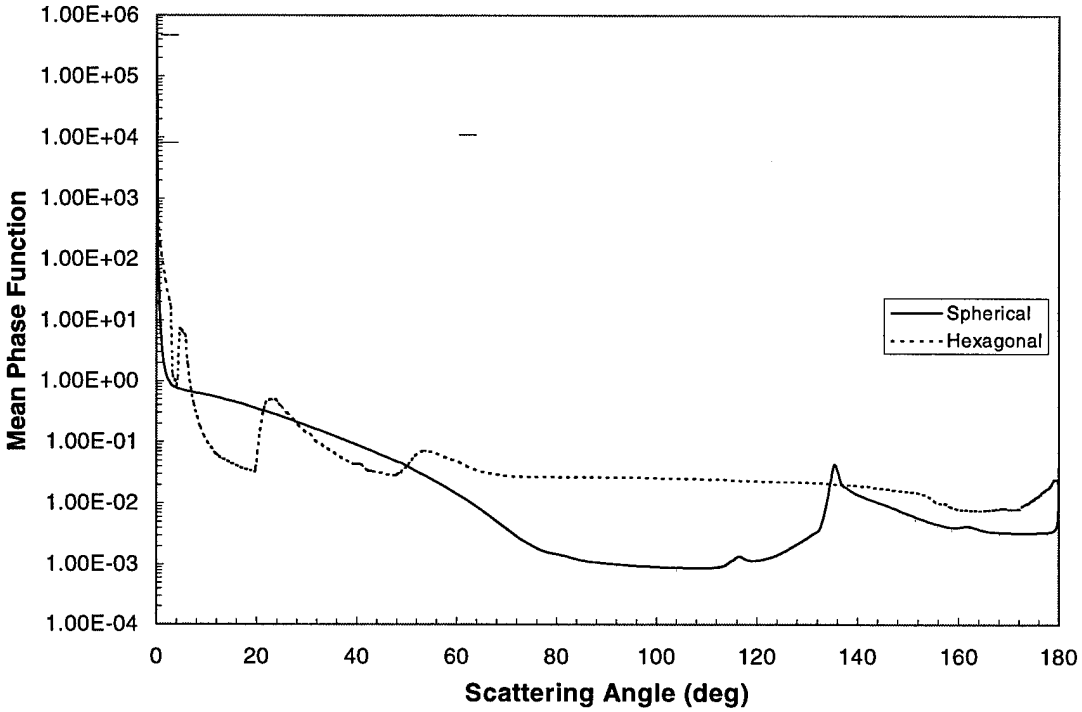

Figure 4.3 Mean phase function as a function of scattering angle for both the spherical and hexagonal approximations.

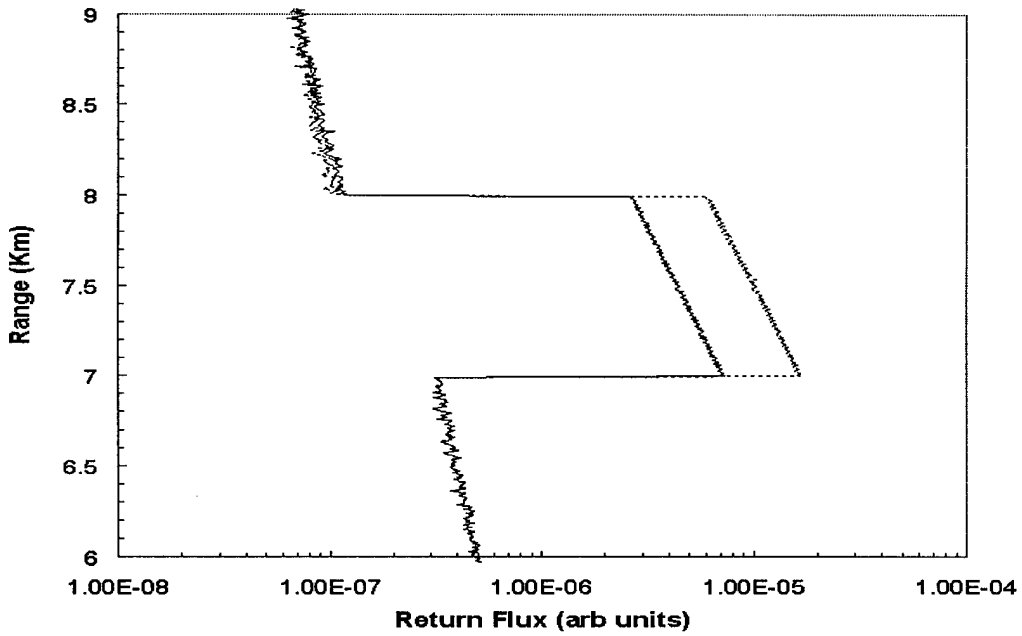

Figure 4.4 Return flux as a function of range for cirrostratus clouds located 7 km above lidar. One cloud is composed of hexagonal crystals (dotted line) and one of spherical crystals (solid line). Liquid water contents set equal so that $\sigma_{ext} = 0.386$ in each cloud. Standard atmosphere is present.

Chapter 5. Results

5.1 Model Returns

Modeling optically thin clouds requires consideration of details that may be neglected when modeling clouds of much greater optical depth. Typical cirrus cloud extinction values are approximately one order of magnitude larger than that of a typical background aerosol and molecular extinction. In contrast, a typical C.1. model cloud (Diermendjian 1969) has extinctions on the order of several hundred times the magnitude of the background extinction. While background Rayleigh and aerosol may be neglected in modeling C.1. type clouds, this is not the case when modeling cirrus clouds. As shown in chapter 2, the background atmosphere increases statistical uncertainty of resolving cloud characteristics and requires the processing of 10 million photons to achieve precision at the 5% level with the current model.

In the presentation of Monte Carlo model profiles, unless otherwise specified, the ordinate in each graph is the range above the lidar in kilometers and the abscissa is the total return flux, or the total probability of photons returning directly to the lidar from each range gate. The return flux is the sum of the probabilities from the first three orders of scattering for each range gate.

Figures 5.1a and 5.1b show total return flux as a function of range for a reference "clear" atmosphere composed of Rayleigh and aerosol scatterers and a 1 km thick cirrostratus cloud composed of randomly oriented hexagonal crystals, respectively. The reference or standard atmosphere return flux is used for calculating volume extinction coefficients using an inversion algorithm described later in this chapter. A model cloud with optical depth equal to 0.386 is easily distinguished from the background atmosphere. This is despite the fact that total flux

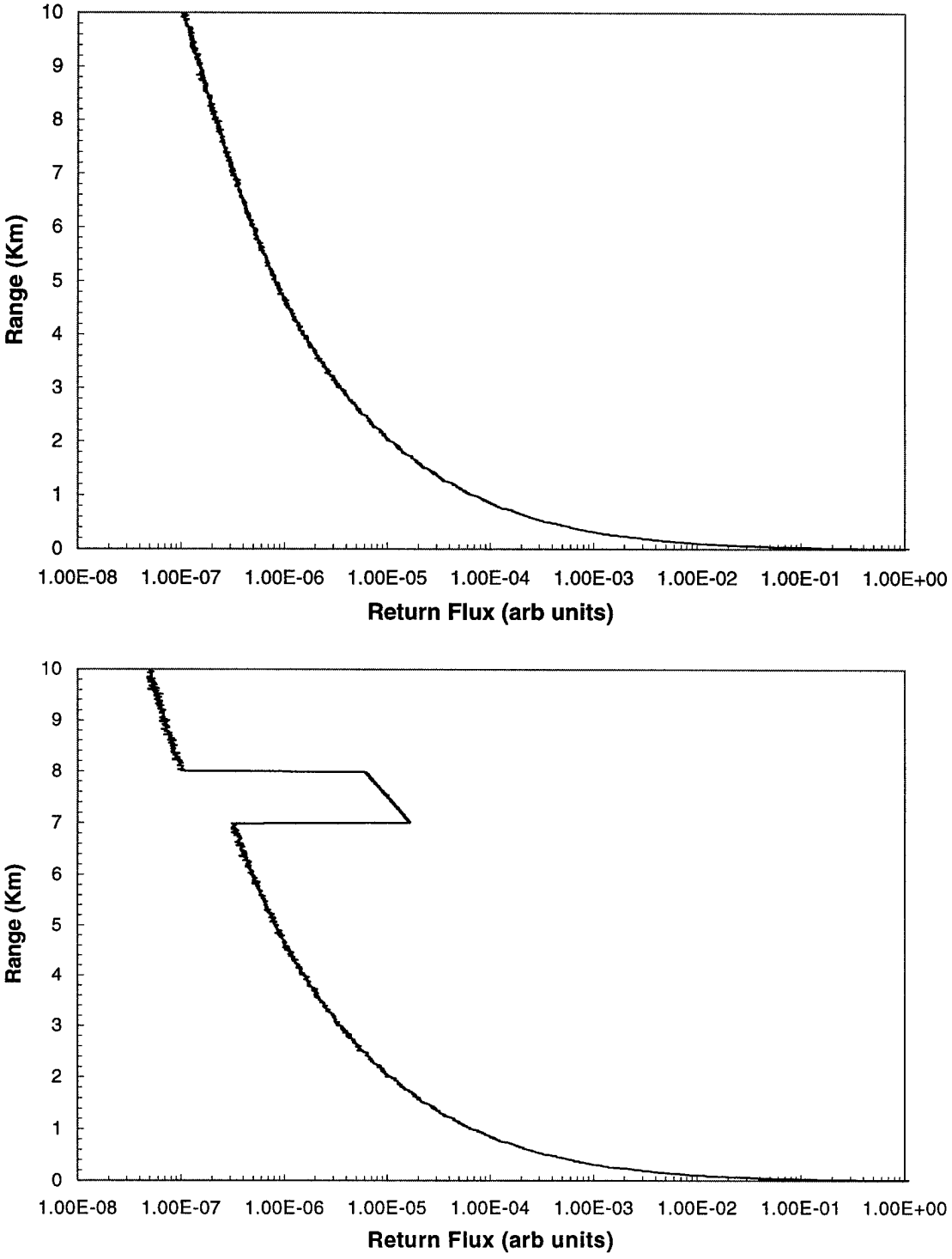

Figure 5.1 Total return flux as a function of range for (a) "clear" atmosphere consisting of standard background Rayleigh and aerosol scattering and (b) 1 km thick cirrostratus cloud composed of hexagonal crystals located 7 km above lidar. Standard atmosphere is present and cloud optical depth is equal to 0.386.

returned from near-ground levels is actually greater than that from the cloud layer. Another characteristic of low cloud optical depth is the ability of photons to penetrate through such a cloud and scatter in the "clear" region above cloud top. This feature allows the analysis of data throughout the cloud and the use of above cloud returns to indicate characteristics about the cloud itself. In contrast, clouds of large optical depth are rarely penetrated more than one-half their geometric depth and no information is obtained from the upper portion or the above cloud region. This limits the researcher's abilities to use return data to infer optical properties of such clouds.

5.2 Determining Cloud Optical Properties

For as long as lidar has been used to sample atmospheric media, researchers have searched for methods that use lidar profiles to determine cloud optical properties. Several techniques have been developed and implemented; however, the validity of the assumptions used in these techniques has been questioned as well as the effectiveness of the techniques themselves. Current model results are used to test some techniques and determine potential for application to real lidar profile data.

A significant step in the search for an effective means of using monostatic single-wavelength lidar returns to extract extinction coefficients was reported by Klett (1981) when he introduced his stable analytical method. The method was based on the premise that by assuming an extinction value at some reference point above cloud level, one could integrate the single scatter lidar equation top down, rather than bottom up. Klett showed that this led to a stable solution. The method relied on the assumption that the volume backscatter and extinction coefficients could be related by the power law,

$$\beta = const * \sigma^k \tag{5.1}$$

where β is the volume backscatter coefficient, σ is the volume extinction coefficient, and k is a form of the backscatter to extinction ratio. By Klett's definition, if *const* is taken to be unity, then $k = \ln \beta / \ln \sigma$, which relates the natural logarithm of backscatter and extinction coefficients. This version of the lidar ratio differs from the more common isotropic backscatter to extinction ratio, $k = \beta/\sigma$ defined by Platt (1981) which is used in this study. Recently, Young (1995) pointed out that Klett's method for deriving cloud optical properties is not satisfactory for optically thin clouds. One reason for this, as discussed by Fernald (1984), is that the lidar ratio $k = \beta/\sigma$, must be known if cloud optical properties are to be found. Platt (1981) showed that k is equal to 4π times the normalized scattering phase function $P(\psi)$ evaluated at π. This relationship is ideally suited for Monte Carlo modeling in which the exact characteristics of cloud hydrometeors are assumed to be known.

The single scattering phase function of typical cirrus clouds is a much debated topic and several theories and calculations have been suggested (Huffman 1970; Jacobowitz 1971; Liou et al. 1976; Takano and Liou 1989). Scattering properties of cirrus clouds have been shown to be dependent on particle habit, size distribution, temperature, and orientation. The use of a widely accepted phase function, such as the one offered by Takano and Liou (1989), is assumed adequate for this study especially since all of the results presented below are presented for relative comparisons.

For this study, a value for k, consistent with Platt (1981), is estimated by using the relationship $\beta_\pi = P(\pi)\sigma_e$ where β_π is the volume backscatter coefficient evaluated at π, $P(\pi)$ is the phase function evaluated at π, and σ_e is the volume extinction coefficient, where absorption is neglected. This leads to lidar ratio $k = P(\pi)$ and makes its determination simple in a controlled model environment. Young (1995) states that the lack of an accurate knowledge of k is a significant problem in the interpretation of lidar measurements of optically thin clouds that is not present in the analysis of thick clouds. He also presents a detailed method of determining

volume backscatter and extinction coefficients from lidar returns, but the method is more general and for a broader range of cloud conditions than needed here. Rather, for this study, the simplified algorithm presented by Alvarez (1993) will be used since it is tailored for use with thin clouds.

5.3 Method

Alvarez, et al. (1993) introduced a technique for extracting cloud optical properties from monochromatic lidar returns. This method is suited for clouds of low optical depths since it provides an effective way of determining the required lidar ratio, k_c, where the subscript c refers to a cloud. It also makes use of signal returns from above cloud top level. The method relies on a more convenient form of the basic single scattering lidar equation introduced in chapter 1. The form makes use of the relation $\beta_\pi = P(\pi)\sigma_e$ and is given by

$$P_r = P_t \frac{A_r \beta_\pi \Delta h}{8\pi r^2} e^{(-2\int_0^r \sigma(r')dr')} \tag{5.2}$$

where P_r is the returned power to the lidar, P_t is the transmitted power, A_r is the effective area of the receiver, β_π is the volume backscatter coefficient, Δh is the laser pulse length, and σ is the volume extinction coefficient. As shown in section 3.3, for MPL operations, single scattering dominates multiple scattering effects for clouds of relatively low optical depth. This further supports the use of equation (5.2). However, it will be shown later that when sampling clouds of greater optical depth, multiple scattering effects may become a significant factor.

An accurate treatment of radiative transfer through low optical depth cloud media must include both molecular and aerosol scattering. With these two factors included, a two component form of the lidar equation is given by

$$P_r = \frac{P_t A_r \Delta h}{8\pi} \frac{\beta_a + \beta_c}{r^2} e^{-2\int_0^r [\sigma_a(r') + \sigma_c(r')] dr'} \tag{5.3}$$

where the subscript a refers to "clear" air composed of aerosol and molecular scatterers and c refers to signal due to cloud hydrometeors. From equation (5.3), a numerical method may be developed to modify the two component equation to yield cloud optical properties. If we acknowledge that a lidar signal composed of power returns or in the case of the current model, return probabilities, is proportional to equation (5.3), we can divide this equation by a return profile from a reference clear atmosphere. In the current model, such a reference return signal was shown in figure 5.1a. As a result of this division, we are left with the attenuated scattering ratio (ASR), R_{sc}. In cloud, this ratio is given by

$$R(r)_{sc} = (1 + \frac{\beta_c}{\beta_a}) e^{-2\int_{r_b}^r \sigma_c(r') dr'} \tag{5.4}$$

where the first term in the integral in equation (5.3) dropped out. The ratio below cloud level is 1 and above cloud, the ASR is given by

$$R_{sc} = e^{-2\int_{r_b}^{r_t} \sigma_c(r') dr'} = e^{-2\tau_e} \tag{5.5}$$

where r_b is cloud base, r_t is the cloud top and τ_e is the cloud optical depth. This equation implies that a direct measurement of cloud optical depth is found from the ratio of lidar return flux above cloud top to the return flux from a corresponding reference "clear" atmosphere. Hereafter, the optical depth found from equation (5.5) will be referred to as estimated cloud optical depth.

To numerically solve equation (5.4), one must assume that the volume backscatter coefficient, β, can be scaled by a density function above a minimum altitude such that

$$\beta(r) = \beta_0 \rho(r) \tag{5.6}$$

where $\rho(r)$ contains altitude dependence of molecular and aerosol number density for altitudes greater than the reference altitude and β_0 is the reference volume backscatter coefficient. To make use of current model parameters, it is convenient to relate $\beta_\pi = P(\pi)\sigma_e$ and equation (5.6) to obtain

$$\beta_0 \rho(r) = \sigma_a P(\pi) \tag{5.7}$$

where $P(\pi)$ for clear air and extinction due to molecular and aerosol scattering, σ_a, are considered to be known quantities such that

$$\sigma_a P(\pi) = \sigma_r P_r(\pi) + \sigma_h P_h(\pi) \tag{5.8}$$

where the subscripts *r* and *h* refer to Rayleigh and haze (aerosol) and $P_r(\pi)$ is 1.5. If we then assume that the cloud lidar ratio, k_c, is a constant, equation (5.4) may be rewritten as

$$R_{sc} = (1+\frac{k_c\sigma_c}{\beta_0\rho(r)})e^{-2\int_{r_b}^{r}\sigma_c(r')dr'} \tag{5.9}$$

where in the current model application, $\beta_0\rho(r)$ is known. Next, if k_c is considered known, σ_c is the only remaining unknown in equation (5.9). It will be shown later that this technique can be expanded to determine k_c. This equation is translated to a numerical equation by dividing the cloud into equal altitude layers and making use of the trapezoid rule to obtain

$$R_{sc(i)} = (1+\frac{k_c\sigma_i}{\beta_0\rho_i})e^{(-\sigma_0\Delta-2\Delta(\sigma_1+\sigma_2+\ldots\sigma_{i-1})-\sigma_i\Delta)} \tag{5.10}$$

where the subscript *i* corresponds to range layers in the cloud with i=0 representing the lowest cloud layer and Δ represents the layer thickness. Calculation is fairly systematic, starting at i=0 where only the extinction σ_0 is present. In this form, equation (5.10) is a transcendental equation and is solved numerically by the bisection method. We now consider σ_1, and since we now know

σ_o, R_1, $\beta_o\rho_1$, and k_c, we solve for σ_1 numerically. If *m* layers are considered, once values of σ_i are known for all *m*, extinction coefficients are summed and what will be called "derived cloud optical depth" is calculated. When solving equation (5.10), note that variables R_{sc} and ρ consist of an array of *m* values. The ASR, R_{sc}, is found directly from model output by comparing the average return probability from a particular cloud layer, i, with the corresponding return from an equivalent "clear" air layer such that

$$R_{sc(i)} = \frac{\sum_{j=1}^{n} RTN_{cld(i)}}{\sum_{j=1}^{n} RTN_{clr(i)}} \tag{5.11}$$

where RTN represents the model return flux output for a particular range gate and *i* represents the atmospheric layer, and *j* is the range gate within each layer consisting of its own value of R_{sc} and ρ. The complexities of determining a suitable value for k_c is a topic of much discussion (Platt 1979, 1981; Young 1995). The advantage of this algorithm is its use of a correlation between the estimated optical depth, τ_e, found from equation (5.5) and the derived optical depth found by solving equation (5.10). If the derived optical depth is substantially different from the estimated optical depth using an assumed value of k_c, the lidar ratio is revised and derived optical depth is recalculated. This process is repeated until the two optical depths are sufficiently close. Therefore, this analysis obtains both the cloud volume extinction array and the lidar ratio, k_c, which can then be used to find optical properties of clouds greater in optical depth.

5.4 Calculations

Results from the Monte Carlo model applied to cirrostratus clouds may be used to investigate the effectiveness of an algorithm to extract both the volume extinction coefficient and cloud optical depth from lidar return signals. The advantage in using model data is that results

can immediately be evaluated. Results will first be presented without consideration of multiple scattering effects.

5.4.1 Homogeneous cirrostratus cloud with randomly oriented hexagonal crystals

The first case studied is a 1 km thick cirrostratus cloud composed of randomly oriented hexagonal crystals at an altitude of 7 km. The modeled cloud returns were shown separately in figures 5.1a and 5.1b and on the same axes in figure 5.2a. In the subcloud region, returns are nearly identical, while in the cloud layer, there exists a differential return flux between returns from "clear" air and cloud profiles. Above the cloud top, returns from the background atmosphere with the cloud present are less than those from a "clear" atmosphere. This difference is the result of an increased extinction by scattering in the cloud; both the lidar pulse incident upon and the backscattered energy from the above-cloud layer suffer extinction by the cloud. Equation (5.5) shows that this differential return from the above-cloud region is proportional to the volume extinction coefficient and hence, the optical depth of the cloud. This differential return provides the ability to estimate cloud optical depth using equation (5.5).

The model cloud extinction coefficient was 0.386 km^{-1} and constant throughout the cloud. The retrieval shown in figure 5.2a resulted in an estimated cloud optical depth of 0.377 using the return from the adjacent 1 km thick layer located above cloud (8-9 km). Taking 4π times $P(\pi)$ for the hexagonal approximation phase function results in k_c equal to 1.18. Using this value of k_c leads to the extinction array shown in figure 5.2b. The derived cloud optical depth of 0.381 compares well with estimated cloud optical depth of 0.377 and the model cloud optical depth of 0.386.

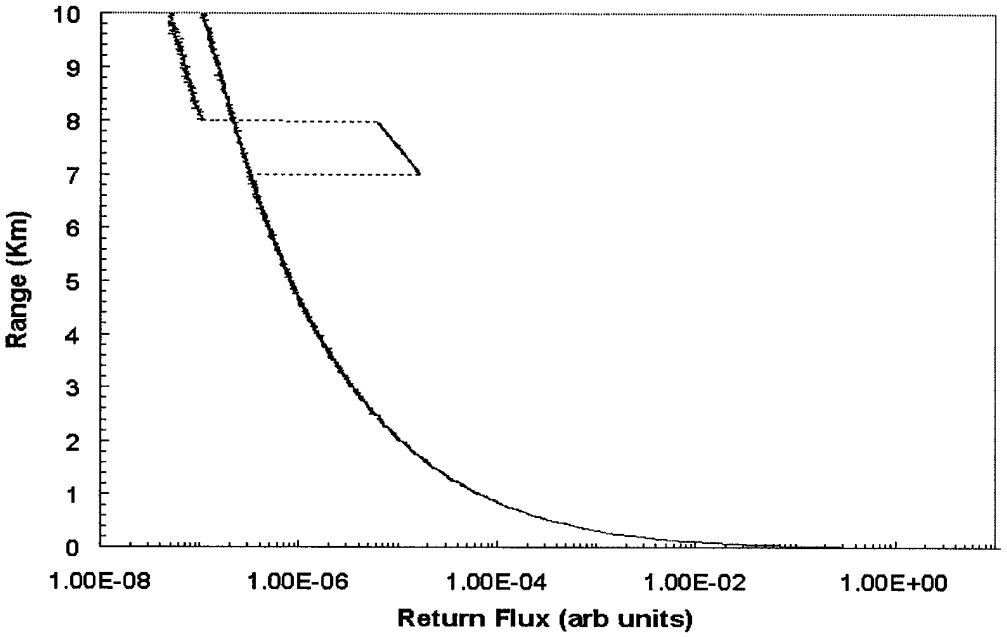

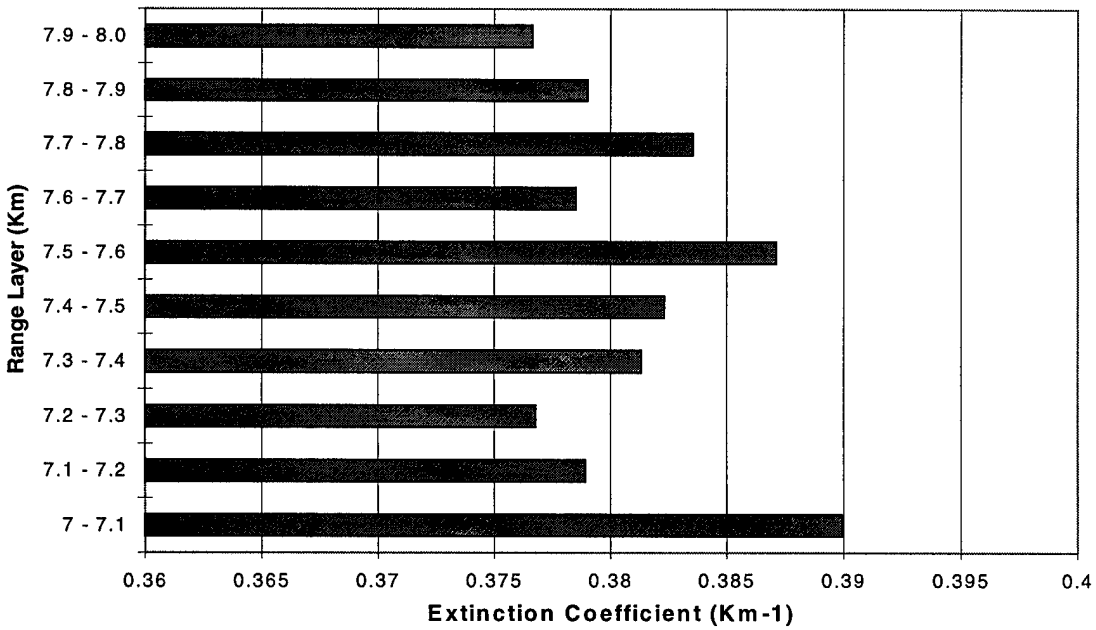

Figure 5.2 (a) "Clear" atmosphere return (dark line) and return from atmosphere including 1 km thick cirrostratus cloud composed of randomly oriented hexagonal crystals located 7 km over lidar (lighter, dotted line). Model cloud optical depth is 0.386. (b) Derived volume extinction coefficient array in 100 m layers. Summation of coefficients leads to a derived cloud optical depth of 0.381.

5.4.2 Homogeneous cirrostratus cloud with twice the extinction

Returns from a cirrostratus cloud with double the liquid water content or twice the extinction are analyzed next. Figure 5.3a shows a comparison of returns from a "clear" atmosphere and a model cloud with an extinction coefficient of 0.772 km^{-1} placed in a standard background atmosphere. In comparison to figure 5.2a, we see a greater cloud return which results in a larger differential return in the cloud layer as well as from the above-cloud layer. The diminished returns from above cloud provide an ASR that leads to an estimated cloud optical depth of 0.779. Again, this compares favorably with a model cloud optical depth of 0.772 and derived cloud optical depth of 0.776 found from a summation of the extinction array shown in figure 5.3b. Variability in the derived layer extinction coefficients is a product of statistical variability in model returns as well as the calculation process. It will be seen that this variability increases as the model cloud optical depth increases.

5.4.3 Cirrostratus cloud with randomly oriented hexagonal crystals and variable extinction

This case is presented to demonstrate the algorithm's ability to detect vertically variable volume extinction coefficients. Figure 5.4a shows returns from both the vertically inhomogeneous cloud and standard background atmosphere. A step pattern is evident due to the variability of the model cloud extinction in 100 meter layers. The estimated cloud optical depth is found to be 0.325, while the derived cloud optical depth from a summation of volume extinction coefficients (shown in figure 5.4b) is 0.326. These values, once again, compare very well with a model cloud optical depth of 0.33. Figure 5.4b shows a comparison of the derived extinction array with the model cloud extinction array and confirms that the optical properties, including vertical structure of the cloud may be inferred using the algorithm.

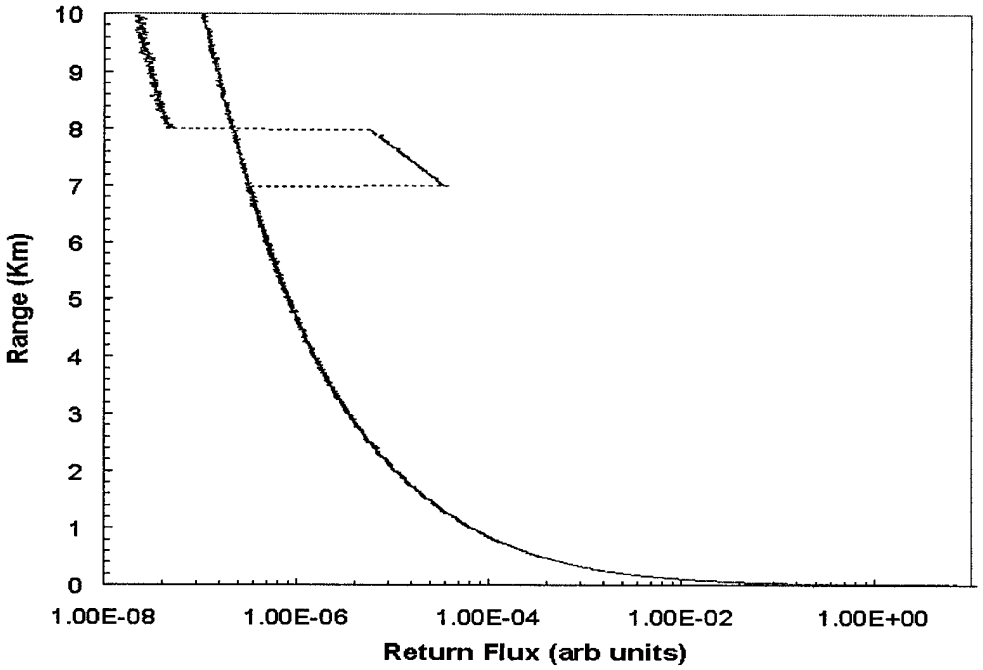

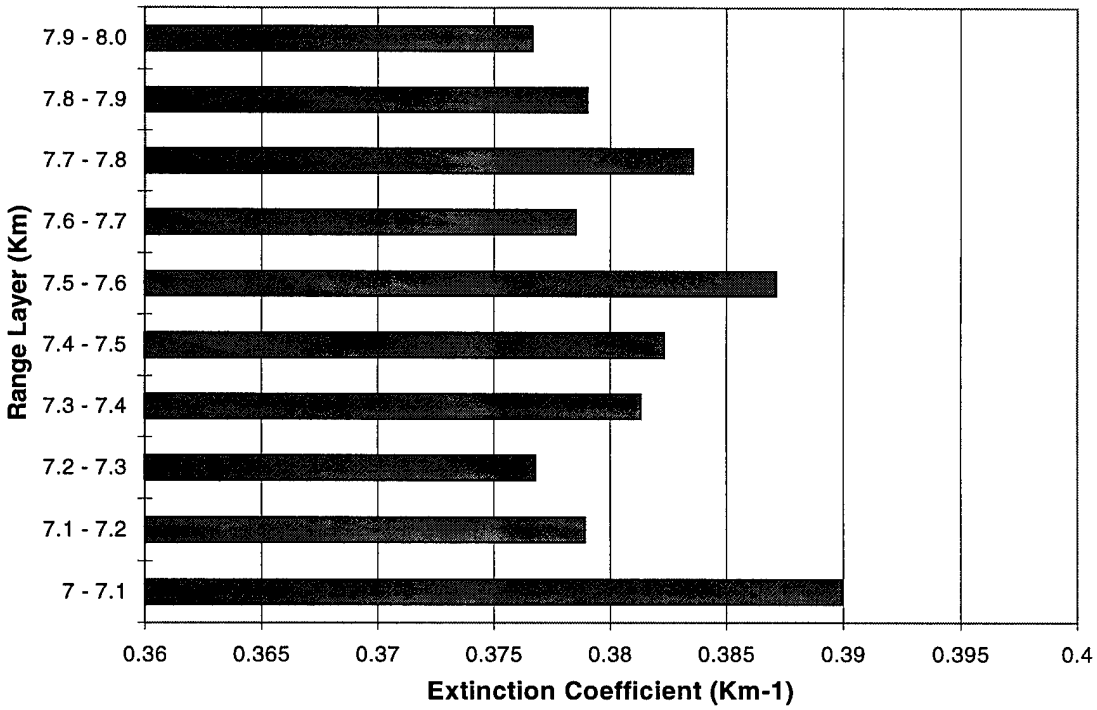

Figure 5.3 (a) Same as figure 5.2a except for twice the extinction and model cloud optical depth equal to 0.772. (b) Derived volume extinction coefficient array for each 100 m layer. Summation of extinction coefficients leads to a derived cloud optical depth equal to 0.776.

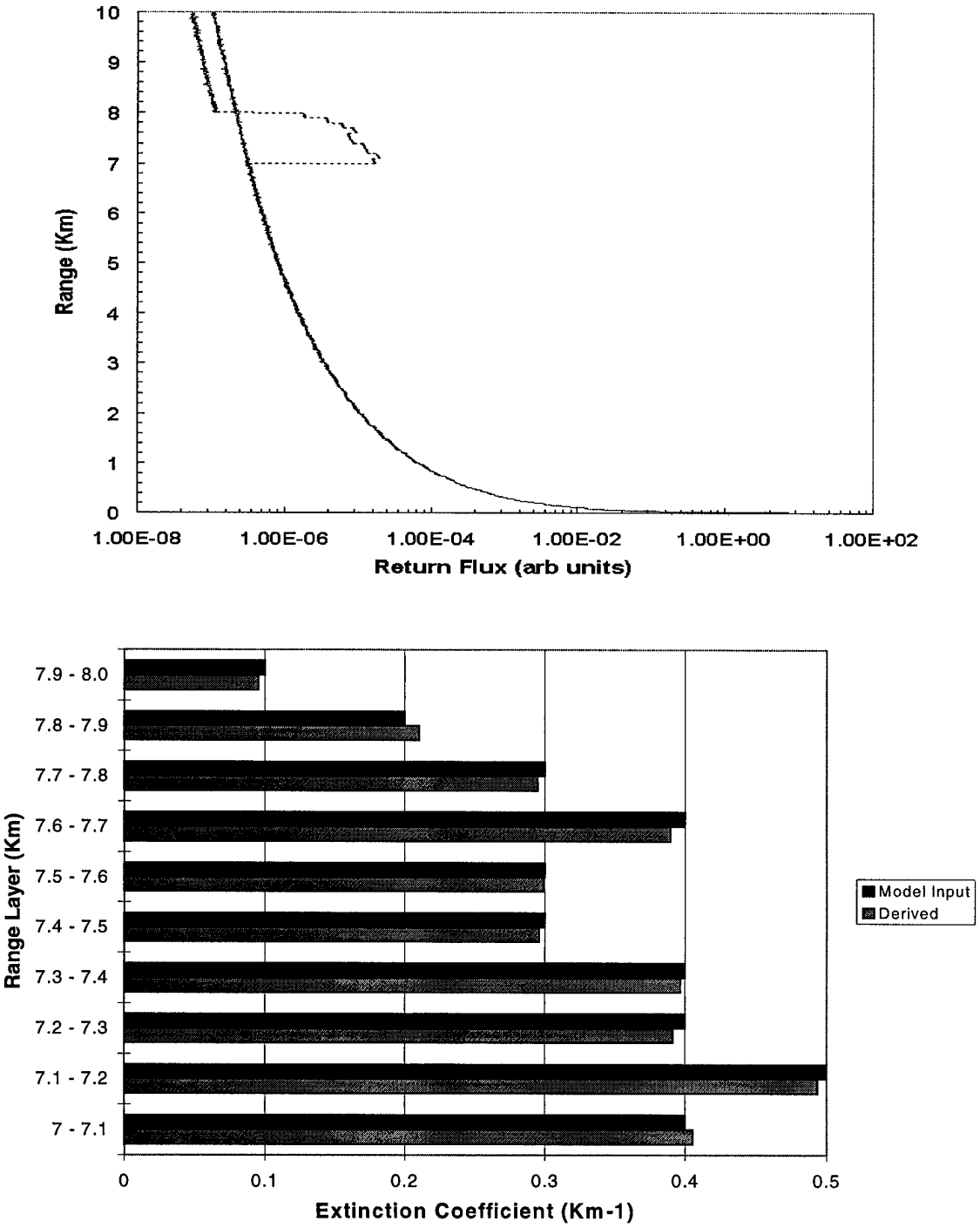

Figure 5.4 (a) Same as figures 5.2a and 5.3a, except now 1 km thick cirrostratus cloud composed of randomly oriented hexagonal crystals contains vertically variable volume extinction coefficients. The model cloud optical depth is 0.33. (b) Comparison of derived with model cloud volume extinction coefficients for each cloud layer.

5.4.4 Optically Thick Cirrostratus Cloud

Next, the algorithm's ability to infer optical properties from a cloud of greater optical depth is tested. A model cloud with an optical depth of 1.54 was specified and results are shown in figure 5.5a. A noticeable increase in return from the cloud layer, compared to earlier results, is evident as well as the corresponding decrease in return from the above-cloud layer. The estimated cloud optical depth was calculated to be 1.51. The calculated volume extinction coefficient array is shown in figure 5.5b. Note the greater variability in the results; statistical uncertainty or "noise" is more prevalent when sampling clouds of greater optical depth. By the algorithm's very nature, any error in the calculations in the lower part of the cloud will result in an accumulation effect as higher layer extinction values are found. As a result, the derived cloud optical depth is found to be 1.67 using k_c equal to 1.18. This shows that in its current form, the algorithm is unable to find agreement between estimated and derived cloud optical depth and fails when modeling clouds of this thickness.

5.5 Limits on Algorithm Applicability

Model returns are used to examine the algorithm's ability to provide accurate estimations of the volume extinction array and cloud optical depth. Given the very nature of the algorithm, its effectiveness is dependent on a few key atmospheric characteristics. First, there must exist a sufficient differential return between cloud and background atmosphere. A cloud with very low optical depth results in cloud returns which are insufficient to produce adequate ASRs in the cloud layer. This leads to increased statistical uncertainty in the algorithm's results. Secondly, an optically thick cloud introduces an increase in photon extinction in the lower portion of the cloud, increased "noise" in Monte Carlo model output, and an increased importance of multiple scattering. All of these factors contribute to the algorithm's unstable behavior. An analysis was conducted to determine effective algorithm maximum and minimum optical depth threshold

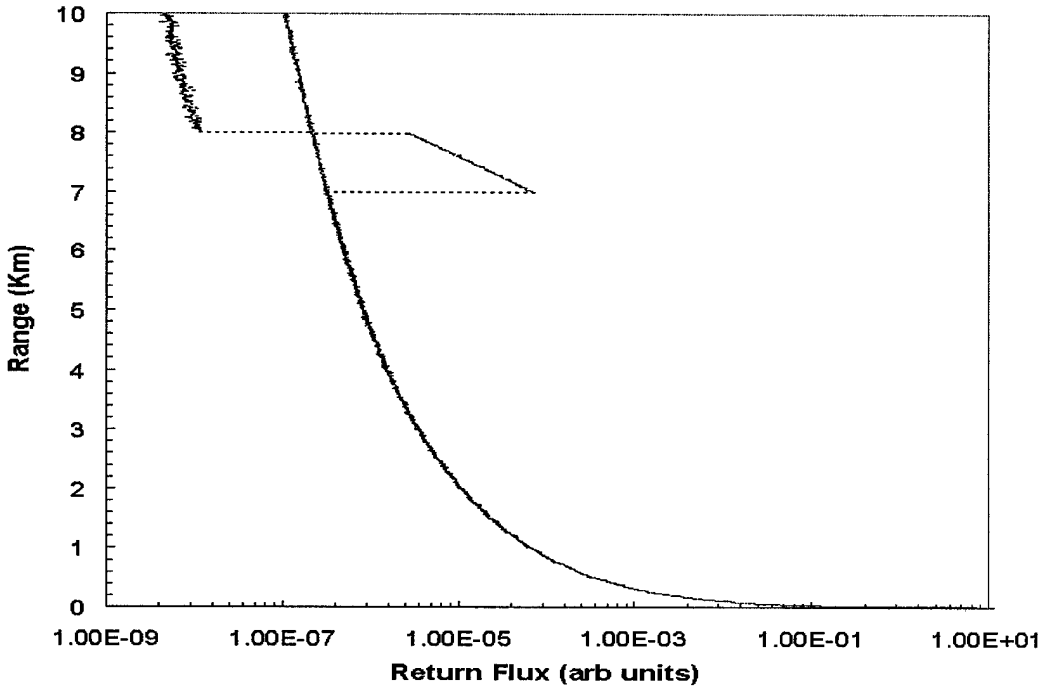

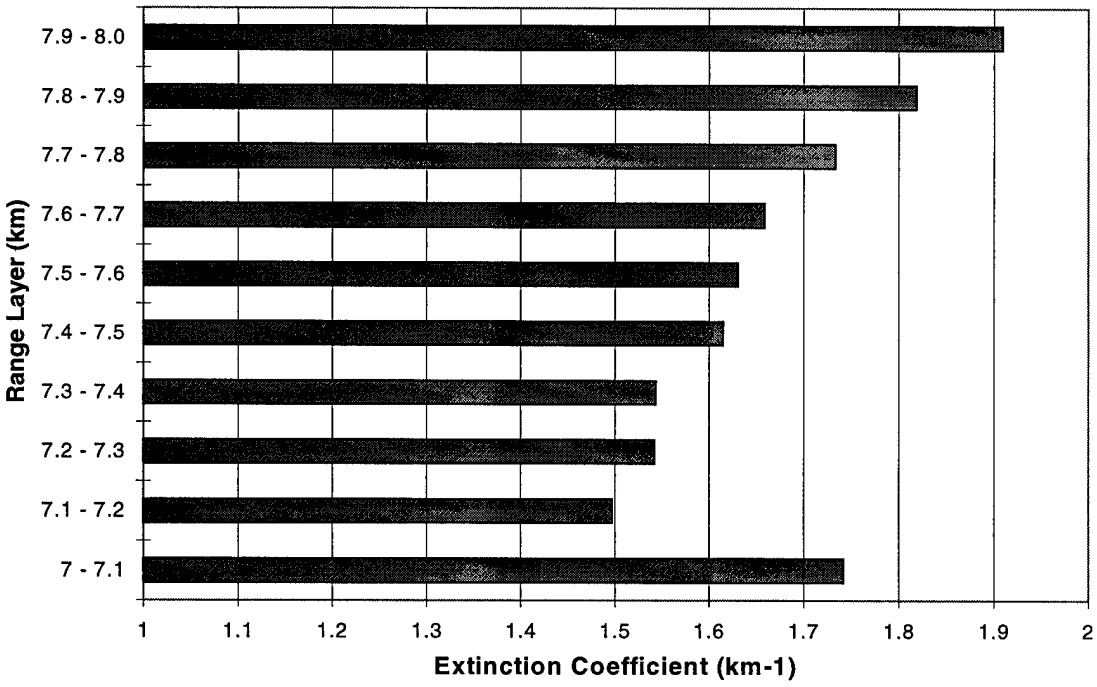

Figure 5.5 (a) Model return profile from homogeneous cirrostratus cloud with model optical depth equal to 1.54. Profile is overlaid on standard background atmosphere return profile. (b) Derived volume extinction coefficient array in 100 m layers. Summation of coefficients leads to a derived cloud optical depth of 1.67.

values. Several model runs were made using homogeneous cirrostratus clouds composed of randomly oriented hexagonal crystals. All simulated clouds are 1 km in depth and located 7 km directly above the lidar. A positive feature of this algorithm is its ability to make two separate calculations of cloud optical depth and then by finding agreement between the two, an effective lidar ratio can be found. This lidar ratio can then be used to determine optical properties of similar clouds. Considering work shown earlier, it is consistent to use a lidar ratio, k_c, of 1.18 in all calculations in which model clouds are composed of the same type crystal habit and orientation.

The effectiveness of the algorithm is contingent on its ability to first estimate the optical depth from the above cloud ASR by calculation of the estimated optical depth and subsequent numerical calculation of the volume extinction coefficient array. The array provides the derived cloud optical depth calculation based on the ASR for each layer within the modeled cloud. The algorithm is considered ineffective when there exists a poor agreement between the two optical depths exists. If k_c is assumed to be known, threshold values can be established based on the algorithm's ability to find sufficient agreement between the estimated and derived cloud optical depths for various model cloud inputs. To determine limits of applicability, a percentage difference, D, is calculated for each model run and is defined as

$$D = \left| \frac{\tau_e - \tau_d}{\tau_e} \right| \times 100 \qquad (5.12)$$

where τ_e is the estimated optical depth found from equation (5.5) and τ_d is the derived optical depth from the calculated extinction coefficient array. Figure 5.6a shows τ_e and τ_d as a function of model cloud optical depth. The solid straight line represents the ideal case in which the algorithm is 100 % accurate and is shown as reference. Figure 5.6b shows D as a function of model cloud optical depth. The algorithm performs well in finding τ_e. Model results showed that

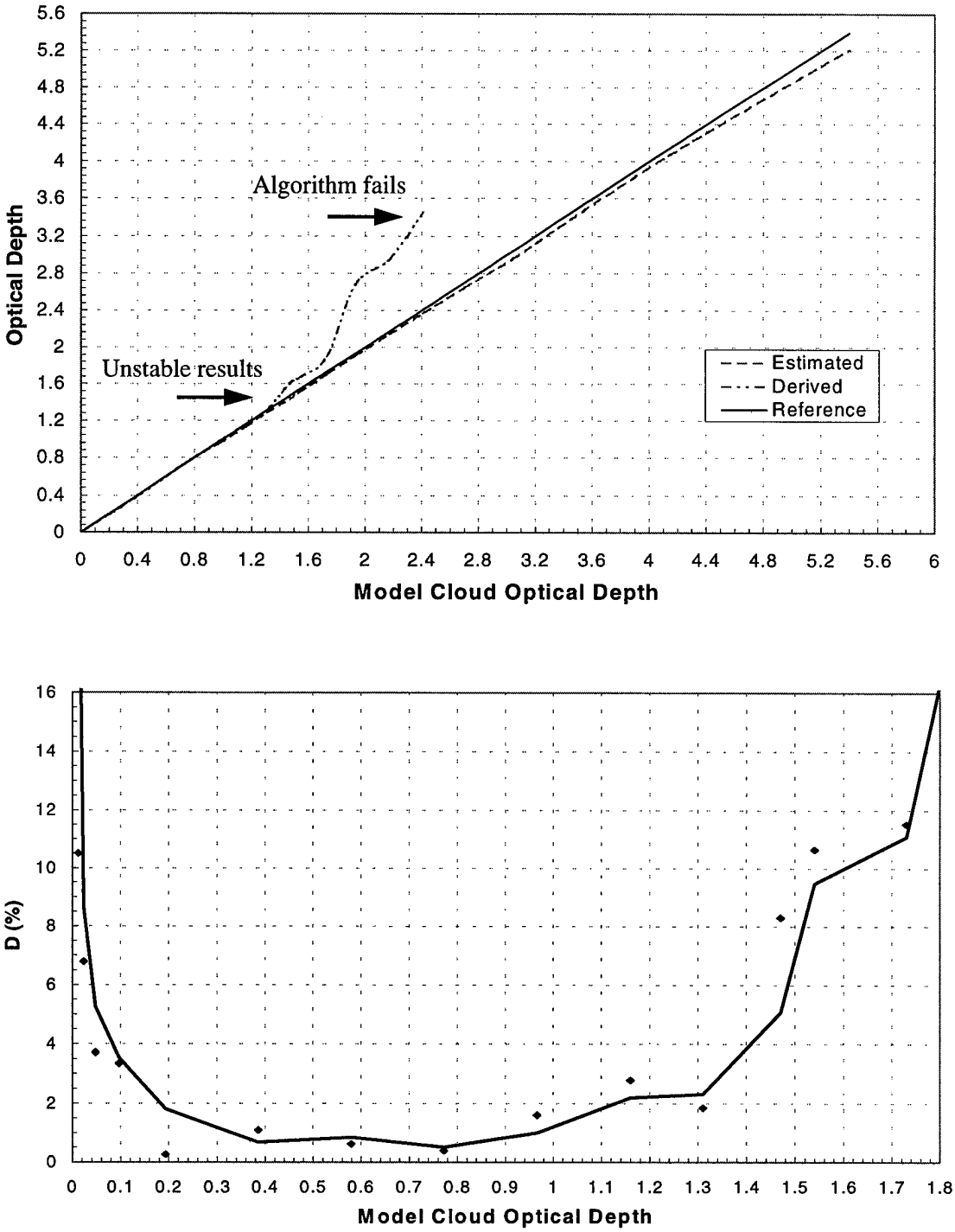

Figure 5.6 (a) Estimated cloud optical depth, τ_e, and derived optical depth, τ_d, as a function of model cloud optical depth. Solid straight line is used for reference. (b) D as a function of model cloud optical depth. Best-fit curve represented by moving average.

a fairly accurate value of τ_e was found up to a model cloud optical depth of about 5.5. Model clouds of greater optical depth, prevent sufficient returns from the above-cloud layer and hence, estimated optical depth can not be found. Even with the success of calculating τ_e, to achieve a value of D less than 5%, the algorithm is bounded by calculations on cloud optical depths that are greater than 0.05 and less than 1.4. Outside this range, calculations become unstable and susceptible to large errors. This results in greater statistical uncertainty and the breakdown of the algorithm's effectiveness due to its inability to achieve a sufficient agreement between τ_e and τ_d. Although accurate values of τ_e are found for higher optical depths, accurate values of τ_d are limited by the algorithm's stability.

5.5.1 Lidar Ratio Variability

Results until now have been based on the assumption that the lidar ratio, k_c, is known. This stems from the use of the known single scattering phase function used to generate model cloud return profiles. As part of a sensitivity analysis, the effect a change in the lidar ratio has on model results was examined. If k_c is unknown, as in the analysis of real lidar data, it may be varied in algorithm calculations until the two cloud optical depth calculations are sufficiently close. At this point, k_c is varied by 1% leading to a new value of derived cloud optical depth. From these two values, the sensitivity of the derived cloud optical depth on the cloud lidar ratio is found. Figure 5.7 is found by changing the derived value of k_c 1% and then examining the subsequent net change in derived cloud optical depth. It can be seen that lidar ratio sensitivity increases steadily as a function of increased model cloud optical depth. Consistent with results given above, if a 5% or greater variability is considered unacceptable, then unstable behavior can be expected when analyzing returns from model clouds with optical depths greater than about 1.4. As before, sufficient agreement cannot be found in model clouds of optical depth less than 0.05.

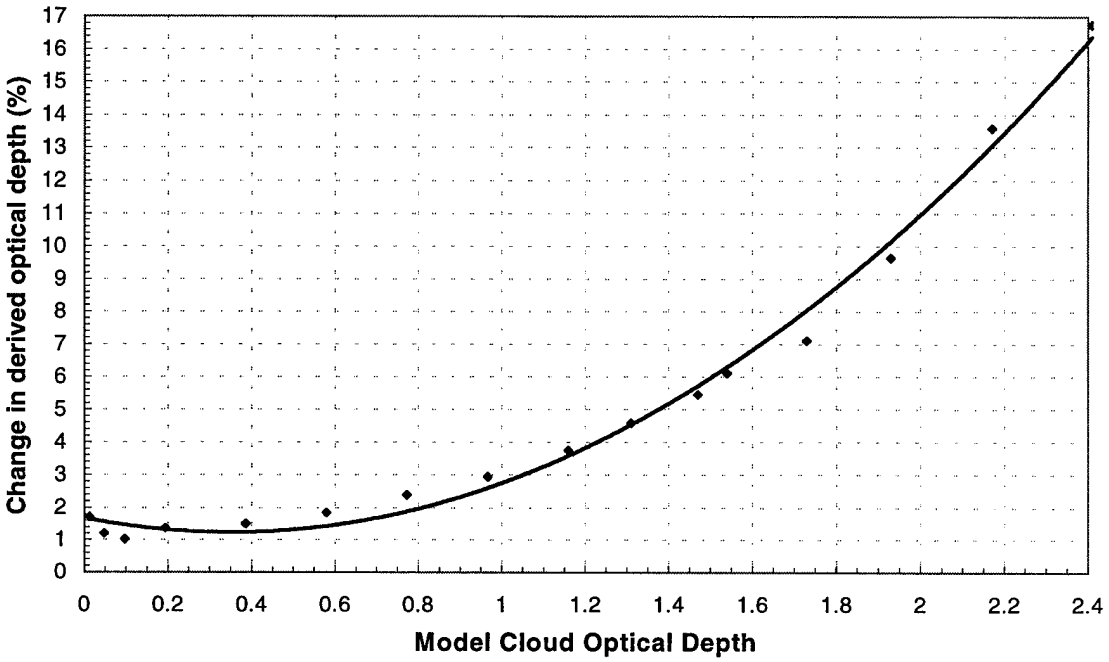

Figure 5.7 Sensitivity of lidar ratio, k_c, as a function of model cloud optical depth. Ordinate represents the percent change in derived optical depth given a 1% change in k_c. Best-fit line represented by second order polynomial.

5.6 Multiple Scattering Factor

Photons that are scattered more than once in the receiver FOV or scattered back into the FOV constitute multiply scattered returns to the MPL. For clouds of low to moderate optical depths, the MPL's small receiver FOV limits the effects of multiple scattering to the point that they may be neglected in algorithm calculations without significant error. Platt (1979, 1981) showed that multiple scattering effects become more pronounced at higher optical depths, deeper penetration into clouds, wider receiver FOVs, greater cloud ranges, and very peaked forward scattering phase functions. Furthermore, when scattering is controlled by such strongly forward peaked phase functions, photons will tend to remain in the receiver FOV, which results in an increased chance of its return to the lidar. Strong forward scattering is a feature of many derived or calculated phase functions used to describe cirrus clouds, including the phase function used in

this work (Takano and Liou 1989). Figure 5.8 compares the contribution multiple scattering has on total return flux in cirrostratus clouds for three model clouds of varying optical depth. The maximum number of scatterers in the Monte Carlo calculations was retained at three. Modeled results showed that even at relatively high optical depths, over 99% of the total return was due to the first three orders of scattering. As in chapter 3, results for a cloud of optical depth equal to 0.386 show that multiple scattering contributes less than 5% of the total return flux. However, as the model cloud is made thicker (i.e. optical depths of 1.31 and 2.41) the contribution of multiple scattering increases through the cloud depth reaching a maximum contribution of approximately 35% for the thickest cloud. Neglecting multiple scattering effects at these levels results could lead to an overestimation of volume extinction and an inaccurate measurement of cloud optical depth.

Febvre (1994) used statistical analysis of in situ microphysical measurements to develop an inversion method for cirrus clouds. Using the standard lidar equation and treating the lidar ratio as a constant, he was able to deduce optical properties of cirrus clouds from lidar return profiles. Febvre neglected multiple scattering effects, but pointed out that unstable behavior of the method was observed with cloud optical depths greater than 1.5. Further, to analyze thicker clouds, it was necessary to introduce a multiple scattering correction factor less than 1. Febvre's findings and those just outlined from the current algorithm, lead to the conclusion that if clouds of greater optical depth are to be analyzed, a multiple scattering correction factor must be included in the calculations.

Platt (1979) introduced a multiple scattering factor η by which the extinction coefficient must be multiplied and which is always less than unity. This factor is required to determine

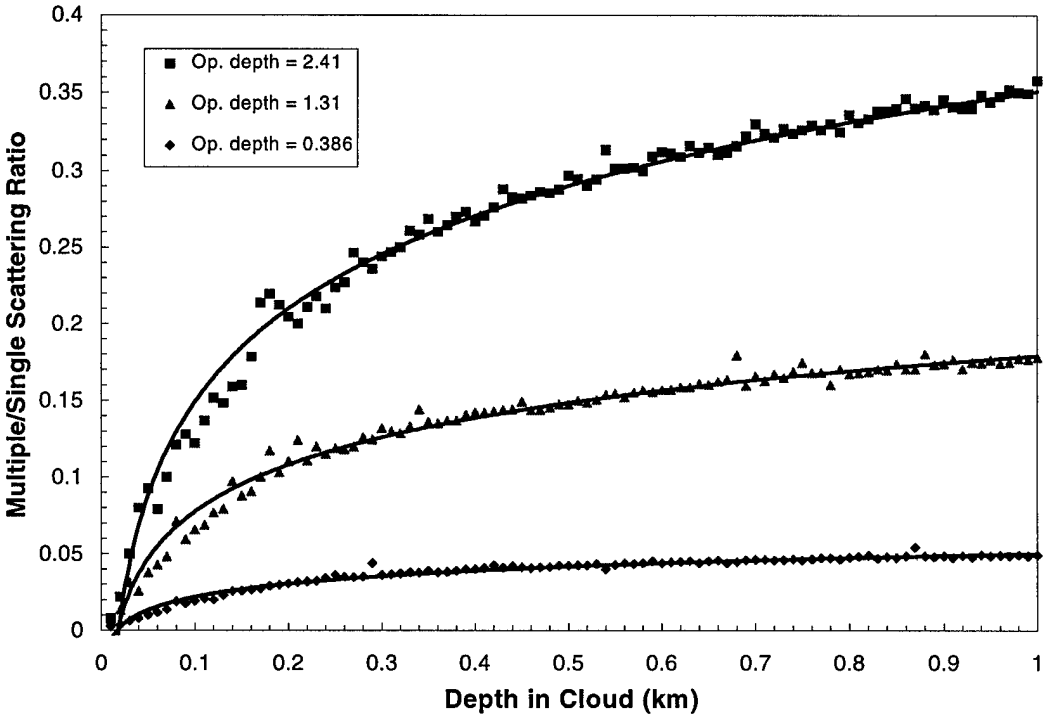

Figure 5.8 Ratio of multiple (second and third order) to single scattering for model cirrostratus clouds of specified optical depths. Best-fit curves represented by logarithmic regression.

optical depth because multiple scattering of photons in the receiver FOV causes more photons to return to the receiver than otherwise would be expected. Not surprisingly, the value of η is dependent on cloud optical depth and depth in cloud. Platt (1981) derived an expression representing the value $\eta(r\text{-}r_0)$ as,

$$\eta(r - r_0) = 1 - \frac{\ln[TS / SS]}{2\tau_c(r - r_0)} \tag{5.14}$$

where $\tau_c(r\text{-}r_o)$ is the cloud optical depth from cloud base r_0 to range r, TS is the total return flux from all orders of scattering, and SS is the return flux from single scattering (η = 1). Use of the Monte Carlo model results and equation (5.14) produced figure 5.9 which shows values of η as a function of depth in cloud for model cirrostratus clouds of optical depths 0.386, 1.31, and 2.41. It is evident that even with the MPL's small receiver FOV, the value of η is a function of cloud

optical depth. Platt (1981) observed that for a given cloud optical depth, $\eta(r)$ is quite sensitive to the receiver FOV. Also, for a given receiver FOV, $\eta(r)$ is sensitive to the cloud optical depth. This was found to be the case for the MPL's FOV of 0.1 mrad, albeit to a lesser degree. Platt (1981) presented Monte Carlo results from a 3 km thick homogeneous cirrus cloud with an extinction coefficient of 1 km^{-1} and cloud base at 6 km. At FOVs equal to 1 and 5 mrad, Platt showed that η varied from about 0.35 (cloud base) to 0.50 (cloud top) and 0.19 (cloud base) to 0.30 (cloud top), respectively. These values are significantly lower than those derived from the current model. This was expected given the MPLs smaller receiver FOV and an optically thinner cloud. In future work, any attempt to model cirrus clouds of relatively large optical depth, must include a multiple scattering factor similar to those shown in figure 5.9.

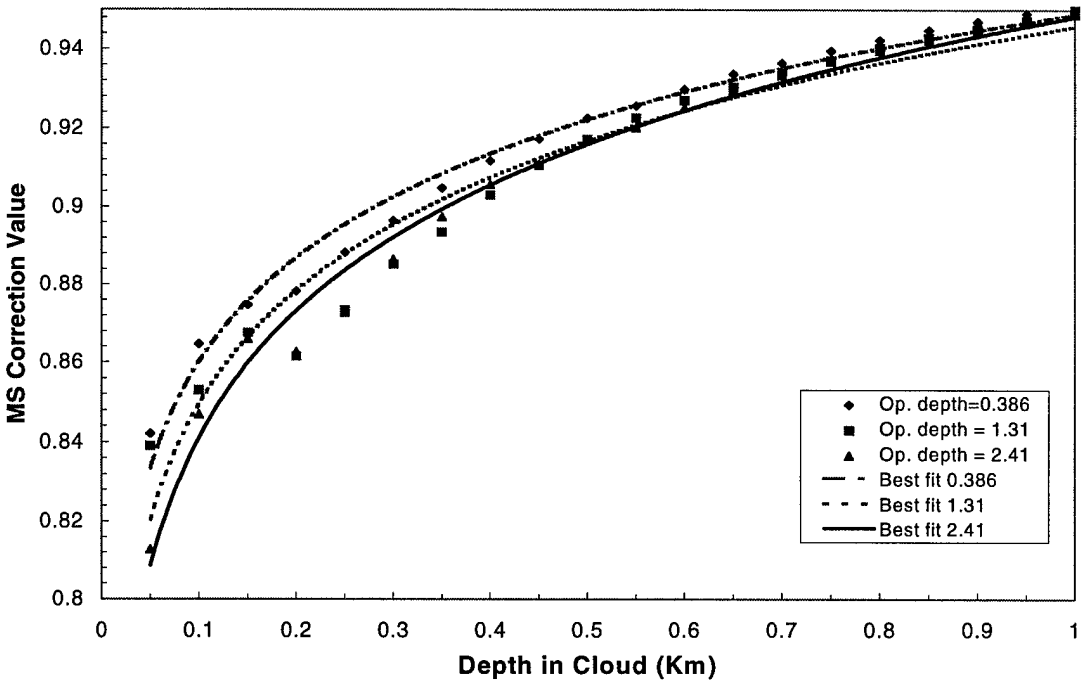

Figure 5.9 Multiple scattering correction value, η, as a function of depth in cloud. Trendlines show best fit approximations to scatter plots of points. Calculations made using model runs of 10 million photons with standard background atmosphere present. Best-fit curves represented by logarithmic regression.

Chapter 6. Conclusions and Future Research Areas

6.1 General Comments

The Micro Pulse Lidar is a relatively new lidar system with the potential to investigate a variety of atmospheric variables. Although the MPL's operating wavelength is in the visible portion of the spectrum, its low energy, high pulse repetition frequency allows for continuous, eye-safe monitoring of the atmosphere. It is shown that at these wavelengths the backscatter from a background atmosphere composed of Rayleigh and aerosol scatterers increases relative to that for near infrared eye-safe lidars. The inclusion of Rayleigh and aerosol scatterers in model calculations significantly increases the statistical uncertainty of the results and requires the processing of an increased number of photons.

The MPL is an effective system for sampling cirrus clouds. Special considerations inherent to sampling optically thin clouds have been identified and investigated by use of a forward Monte Carlo model. The sensitivity of MPL returns to the backscattering characteristics of the model cloud is presented. The treatment of cirrus crystals as spherical particles leads to a misrepresentation of their scattering and absorption properties (Takano and Liou 1989). A better representation is found when single scattering properties of randomly oriented hexagonal crystals are used.

Total return flux from model cirrostratus clouds were examined and the results were shown. Optically thin cirrus clouds enable one to infer radiative properties through the depth of the cloud as well as in the above-cloud region. This is not possible when sampling clouds of greater optical depth. An inversion algorithm first presented by Alvarez et al. (1993) was stated, developed further, and tested. The algorithm was redesigned to use Monte Carlo model output

directly to infer optical properties of the model cirrostratus clouds. The ratio of the lidar return profile with cloud present to the return profile from a reference "clear" atmosphere was defined as the attenuated scattering ratio (ASR). Two independent estimates of cloud optical depth were found. First, the estimated cloud optical depth was deduced directly from the above-cloud ASR. Second, the derived cloud optical depth measurement was found by use of the trapezoid rule which divides the cloud optical depth integral into an equal number of atmospheric layers. In this application, it was necessary to assume that the cloud lidar ratio, k_c, was a constant through the cloud. An iterative procedure in which k_c was allowed to vary while holding everything else constant, was used to identify an effective cloud lidar ratio. The algorithm worked well for model clouds of optical depths greater than 0.05 and less than 1.4. Outside this range, results became unstable due to "noise" in model results and potential multiple scattering effects.

Platt (1981), Febvre (1994), and Young (1995) reported results about the role multiple scattering plays in both the detection of cirrus clouds and the retrieval of optical properties from lidar returns. In an effort to limit the amount of background radiation by making the MPLs receiver FOV as small as possible, the significance of multiple scattering effects significantly diminished except when sampling clouds of relatively large optical depths. Values of multiple scattering correction factor, η, were found by use of a relationship first introduced by Platt (1979). It was found that the MPLs relatively small receiver FOV caused derived values of η to be much higher than those given by Platt. This is an important factor that must be considered in any future profiling of MPL data.

Simulated Monte Carlo lidar returns are incorporated into the inversion algorithm to investigate the retrieval of several important cloud optical properties. The cloud lidar ratio, k_c, can be found by finding an agreement between two separate measurements of cloud optical depth. Volume extinction coefficients may be inferred throughout the depth of the cloud. It is shown that vertical inhomogeneities can be detected. Also, optical depth estimations found from

the above-cloud ASR were shown to provide accurate results for model clouds with optical depths as large as 5.5. These results have the potential to be used in the analysis of real world lidar return profiles. Several significant questions remain unanswered; a few of these topics are described in the next section.

6.2 Future Research Areas

6.2.1 Polarization Studies

Historically, polarization of emitted laser energy has been used to determine the phase of hydrometeors. As pointed out in a review article by Sassen (1991) , researchers have been able to find insights into cloud hydrometeors by examining the depolarization of incident lidar pulse energy. Sassen states that spherically symmetrical scatterers such as drizzle or cloud drops, generate no depolarization of the incident energy, while scatterers with arbitrary geometry, such as ice particles, should generate copious amounts of depolarization. This technique can be duplicated by the MPL with the addition of necessary hardware. To model such effects requires revisions to the current model that were not addressed in this work. In modeling cirrus clouds and their interaction with emitted lidar energy, it is common to assume clouds are completely glaciated and only ice crystals exist. However, in situ observations from the first ISCCP regional experiment (FIRE) produced evidence that substantial liquid water can exists in cirrus clouds at temperatures less than -40°C (Mitchell et al. 1993). This would have an impact on the cloud's radiative properties and well suited for investigation by the use of polarization techniques.

6.2.2 Ice Crystal Orientation

Polarization techniques can also be used to examine ice crystal orientations. Many of the most widely used published phase functions for hexagonal ice crystals (Takano and Liou 1989) are for randomly oriented crystals. Therefore, when modeling a cloud volume, exact incident angle of the photon is not essential to achieve accurate results. However, it has long been theorized that a crystal's long axis is aligned in the horizontal creating a horizontal bias. Wendling et al. (1979) presented a phase function for crystals of horizontal orientation. Results showed that increased backscatter radiation can be expected given a further backward peak in the single scattering phase function. Platt et al. (1977) presented observational results which suggested that by changing the lidar's transmission zenith angle by just 0.5°, a decrease in backscatter intensity of about 3% was observed from the zenith value. At 2°, a decrease of an order of magnitude was observed. Additionally, the change resulted in an increase in the depolarization ratio. The examination of these two lidar derived parameters leads many to believe that a preferred crystal orientation does exist.

The modeling of crystals with a horizontal orientation presents problems which do not exist when modeling clouds which are assumed to be composed of randomly oriented hexagonal crystals. This treatment complicates the interaction between the modeled photon and cloud volumes. A horizontally oriented phase function is for hexagonal ice columns oriented in a plane with the incident radiation normal to the crystal's c-axis. Therefore, the phase function is specifically valid for single scattering from a vertically pointing lidar. Higher orders of scattering must be represented by a phase function which, in essence, is geometrically dependent. In other words, once the incident radiation, or photon, is no longer incident normal to the c-axis, the phase function is no longer specifically valid. This complication is even more pronounced when considering a non-vertically pointing lidar. As in Platt et al. (1977), if the current model were to be revised to allow for elevation angles less than 90°, the same geometric dependence

would exist for single scattering as well. A problem exists in that for every order of scattering, the incident angle with respect to the crystal's orientation must be known. Once it is known, an appropriate phase function must be chosen to produce a probability density function used to predict an effective scattering angle.

References

Alvarez, J.M., M.P. McCormick, and M.A. Vaughan, 1993: A numerical technique for the calculation of cloud optical extinction from lidar. *Fire Cirrus Science Conference Proceedings*, 14-17 Jun 93, 62 - 65.

Bruscaglioni, P., A. Ismaelli, and G. Zaccanti, 1995: Monte-Carlo calculations of lidar returns: Procedure and results. *Applied Physics B*, **60**, 325-329.

Carswell, A. I., A. Fong, S. R. Pal, and I. Pribluda, 1995: Lidar-derived distribution of cloud vertical location and extent. *J. of Applied Meteorology*, **34**, 107-120.

Deirmendjian, D., 1969: **Electromagnetic Scattering on Spherical Polydispersions**, Elsevier, 290 pp.

Elterman, L., 1968: UV, visible, and IR attenuation for altitudes to 50 km, Technical Report AFCRL-68-0153.

Febvre, G., 1994: Lidar data inversion for cirrus clouds: An approach based on a statistical analysis of in situ microphysical measurements. *J. of Atmospheric and Oceanic Technology*, **11**, 1231-1241.

Fernald, F. G.,1984: Analysis of atmospheric lidar observations: some comments. *Applied Optics*, **23**, 652 - 653.

Huffman, P., 1970: Polarization of light scattered by ice crystals. *J. of the Atmospheric Sciences*, **27**, 1207-1208.

Jacobowitz, H., 1971: A method for computing the transfer of solar radiation through clouds of hexagonal ice crystals. *J. Quant. Spectros. Radiative Transfer*, **11**, 691-695.

Keith, C. W. and S. K. Cox, 1994: Monte-Carlo modeling of multiply scattered laser ceilometer returns, M.S. Thesis, Colorado State University, Paper #548.

Klett, J.D., 1981: Stable analytical inversion solution for processing lidar returns. *Applied Optics*, **20**, 211 - 220.

Klett, J.D., 1984: Lidar inversion with variable backscatter/extinction ratios. *Applied Optics*, **24**, 1638 - 1643.

Kunkel, K. E. and J. A. Weinman, 1976: Monte Carlo analysis of multiply scattered lidar returns. *J. of the Atmospheric Sciences*, **33**, 1772-1781.

McCormick, M. P. et al., 1993: Scientific investigations planned for the lidar in-space technology experiment (LITE). *Bulletin of the American Meteorological Society*, **74**, 205-214.

McKee, T. B. and S. K. Cox, 1974: Scattering of visible radiation by finite clouds. *J. of the Atmospheric Sciences*, **31**, 1885-1892.

McKee, T. B. and S. K. Cox, 1976: Simulated radiance patterns for finite cubic clouds. *J. of the Atmospheric Sciences*, **33**, 2014-2020.

Mitchell, D. L., et al., 1993: Are tropical cirrus brighter than mid-latitude cirrus? *Fire Cirrus Science Conference Proceedings*, 14-17 Jun 93, 188-190.

Pal, S. R., W. Steinbrecht, and A. I. Carswell, 1992: Automated method for lidar determination of cloud-base height and vertical extent. *Applied Optics*, **31**, 1488-1494.

Pal, S. R., A. I. Carswell, I. Gordon, and A. Fong, 1995: Lidar-derived cloud optical properties obtained during the ECLIPS program. *J. of Applied Meteorology*, **34**, 2388 - 2399.

Plass, G. N. and G. W. Kattawar, 1968: Radiative transfer in water and ice clouds in the visible and infrared regions. *Applied Optics*, **10**, 738-749.

Platt, C. M., 1979: Remote sounding of high clouds: I. Calculation of visible and infrared optical properties from lidar and radiometer measurements. *J. of Applied Meteorology*, **18**, 1130-1143.

Platt, C. M., 1981: Remote sounding of high clouds. III: Monte Carlo calculations of multiple-scattered lidar returns. *J. of the Atmospheric Sciences*, **38**, 156-167.

Platt, C. M. and A. C. Dilley, 1981: Remote sounding of high clouds. IV: Observed temperature variations in cirrus optical properties. *J. of the Atmospheric Sciences*, **38**, 1069-1082.

Platt, C. M. et al, 1994: The experimental cloud lidar pilot study (ECLIPS) for cloud-radiation research. *Bulletin of the American Meteorological Society*, **75**, 1635-1654.

Sassen, K. and K. N. Liou, 1979: Remote sounding of high clouds: I. Calculations of visible and infrared optical properties from lidar and radiometer measurements. *J. of Appl. Meteor.*, **18**, 1130-1143.

Sassen, K., 1991: The polarization lidar technique for cloud research: A review and current assessment. *Bulletin of the American Meteorological Society*, **72**, 1848-1866.

Spinhirne, J. D., 1993: Micro Pulse Lidar. *IEEE Trans. Geosc. Rem. Sens.*, **31**, 48-55.

Takano, Y. and K. N. Liou, 1989: Solar radiative transfer in cirrus clouds. Part I: Single-scattering and optical properties of hexagonal ice crystals. *J. of the Atmospheric Sciences*, **46**, 3-19.

Winker, D. M. and L. R. Poole, 1995: Monte-Carlo calculations of cloud returns for ground-based and space-based Lidars. *Applied Physics B*, **60**, 341-344.

Young, S.A., 1995: Analysis of lidar backscatter profiles in optically thin clouds. *Applied Optics*, **34**, 7019 - 7031.